A signalling-regulated short-chain dehydrogenase of *Stagonospora nodorum* regulates asexual development

Kar-Chun Tan[1], Joshua L. Heazlewood[2,3], A. Harvey Millar[2], Gordon Thomson[4], Richard P. Oliver[1] and Peter S. Solomon[1*]

[1]*Australian Centre for Necrotrophic Fungal Pathogens, SABC, Faculty of Health Sciences, Murdoch University, Murdoch 6150, Australia.* [2]*Australian Research Council Centre of Excellence in Plant Energy Biology, The University of Western Australia, Crawley 6009, Australia.* [4] *School of Biological Sciences and Biotechnology, Division of Science and Engineering, Murdoch University, Murdoch 6150, Australia.*

*Corresponding author. Mailing address: ACNFP, FHS, Murdoch University, South Street, Murdoch 6150, Australia. Phone: +61 8 9360 7239. Fax: +61 8 9310 4144. E-mail: p.solomon@murdoch.edu.au

[3] Current address: Joint Bioenergy Initiative, Lawrence Berkeley Laboratories, CA, USA.

Running title: Sporulation in *S. nodorum*

ABSTRACT

The fungus *Stagonospora nodorum* is a causal agent of leaf and glume blotch disease of wheat. It has been previously shown that inactivation of heterotrimeric G protein signalling in *Stagonospora nodorum* caused development defects and reduced pathogenicity [Solomon *et al. Mol. Plant-Microbe Interact.* 2004, *17*, 456-466]. In this study, we sought to identify targets of the signalling pathway that may have contributed to phenotypic defects of the signalling mutants. A comparative analysis of the *Stagonospora nodorum* wildtype and a Gα-defective mutant (*gna1*) intracellular proteomes was performed via two dimensional-polyacrylamide gel electrophoresis. Several proteins showed significantly altered abundances when comparing the two strains. One such protein, the short-chain dehydrogenase Sch1, was 20-fold less abundant in the *gna1* strain implying it is positively regulated by Gα signalling. Gene expression and transcriptional enhanced-GFP fusion analyses of *Sch1* indicates strong expression during asexual development. Mutant strains of *Stagonospora nodorum* lacking *Sch1* demonstrated poor growth on minimal media and exhibited a significant reduction in asexual sporulation on all growth media examined. Detailed histological experiments on *sch1* pycnidia revealed the gene is required for the differentiation of the sub-parietal layer of asexual pycnidia resulting in a significant reduction in both pycnidiospore size and numbers.

INTRODUCTION

The heterotrimeric G protein family is a universal eukaryotic signalling component. The heterotrimer consists of α, β and γ subunits that are coupled to the cytoplasmic side of a membrane-bound G protein coupled receptor (GPCR). The binding of a ligand to the GPCR causes exchange of GDP for GTP on the Gα subunit unit resulting in its dissociation from the Gβγ complex. The released Gα subunit can then activate downstream cellular effectors [1, 2]. Four different classes of mammalian Gα proteins have been proposed based on amino acid sequence relationship [3]. The $G\alpha_s$ and $G\alpha_i$ classes function to stimulate and inhibit cyclic AMP production respectively, whereas $G\alpha_q$ subunits function within the phosphotidylinositol pathway and $G\alpha_{12/13}$ activates signalling through the small Rho GTPase [3, 4].

The roles of heterotrimeric G proteins in plant pathogenic fungi have been extensively studied [5, 6]. At least 23 Gα genes of plant pathogenic fungi have been reported in the literature thus far. These 23 genes can be subdivided into two groups related to the mammalian $G\alpha_s$ and $G\alpha_i$ proteins based on the amino acid sequences [5]. Mutants that are impaired in $G\alpha_i$ subunits often possess significant phenotypic defects that can affect the fitness of the pathogen [7-16], implying that this signal transduction system controls processes vital for pathogenicity (Table 1). Transcriptomics has been used to elucidate targets of $G\alpha_i$ subunit signalling in the gray mold *Botrytis cinerea* and the chestnut blight fungus *Cryphonectria parasitica*. These studies have shown signalling regulation of the botrydial toxin gene *Bcbot1* in *B. cinerea* [17, 18] and hypovirus-responsive genes in *C. parasitica* [19], respectively.

Proteomic approaches provide a complementary means of identifying targets of G protein signalling. Previously, such approaches have been used to study phytopathogenic fungi

through protein profiling [20-24] and to identify host- [25] and morphogenesis-responsive proteins [26]. Recent sequencing of the genomes of the phytopathogenic fungi *Magnaporthe grisea, Ustilago maydis, Fusarium graminearum* and *Stagonospora nodorum* [27-30] provides an opportunity for more thorough mass spectrometry-based proteomic analyses [23, 24].

Stagonospora nodorum is a major fungal pathogen of wheat [31]. The role of signal transduction in the pathogenicity of *S. nodorum* has been recently scrutinised [7, 32, 33]. Of particular interest were strains harbouring an impaired Gα gene, *Gna1*. Mutants were reduced in their ability to colonise the host, failed to sporulate, showed an albino phenotype and reduced extracellular depolymerase activities. It was hypothesised that these impairments were a result of changes in the state or abundance of heterotrimeric G protein signalling targets. The aim of this experiment was to identify and functionally characterise proteins regulated by the Gna1 protein using two dimensional-polyacrylamide gel electrophoresis (2D-PAGE). This proteomic approach has led to the identification of several proteins regulated by Gna1 signalling including Sch1, a short-chain dehydrogenase that is positively regulated. Subsequent genetic dissection of *Sch1* revealed it has a required role in asexual development, a critical facet of disease for this polycyclic pathogen.

MATERIALS AND METHODS

Gene nomenclature. The nomenclature of all *S. nodorum* genes mentioned in this study are denoted by the prefix 'SNOG' used in conjunction with the designated gene number. Details of the version 1 annotated sequenced genome can be found at NCBI; http://www.ncbi.nlm.nih.gov/entrez/viewer.fcgi?db=nuccore&id=62183523.

Growth and maintenance of *Stagonospora nodorum*. *S. nodorum* SN15 wildtype (Department of Agriculture, Western Australia) and the *gna1-35* strain carrying a disruption in *Gna1* (Genbank accession number, EAT82421) were used in this study and were maintained on complex media as described [7]. For the analysis of the intracellular proteome, 150 mg of fungal mycelia were grown in minimal medium (MM) broth (pH 6.0) which consisted of 30 $g.L^{-1}$ glucose as a carbon source. The fungus was grown to a vegetative phase by incubation at 22^{o}C shaking at 150 rpm for three days. Mycelia were harvested and freeze-dried overnight.

Growth and maintenance of wheat. Growth of *Triticum aestivum* (cv. Amery) and wheat infections were performed as previously described [7].

Protein extraction. For intracellular proteins, freeze-dried mycelia were homogenised with a cooled mortar and pestle with 10 mM Tris pH 7.6 and 1 mM PMSF. Glass beads (106 μm) of equal volume to the mycelia were used to assist tissue grinding. The crude homogenate was collected and centrifuged at 20,000 *g* for 1 h at 4^{o}C. The resulting supernatant was retained and incubated with 20 units of DNase and 20 units of RNase for 1 h at 25^{o}C. Following this, proteins were precipitated with nine volumes of ice-cold acetone. Precipitated proteins were collected by centrifugation at 4,000 *g* for 15 min at 4^{o}C and washed with 90% ice-cold acetone. Precipitated proteins were solubilised with multiple surfactant solution (MSS) which consisted of 40 mM Tris, 2% (w/v) CHAPS, 2% (w/v) SB

3-10, 5 M urea, 2 M thiourea, 2 mM tributylphosphine (Bio-Rad), 0.2% (v/v) Bio-Lyte 3-10 (Bio-Rad) and 0.002% (w/v) bromophenol blue (Bio-Rad). A probe tip Misonix Sonicator XL2015 set to an output of 95 W and a 25%.s^{-1} pulsar duty cycle was used to assist in protein solubilisation. Unless denoted otherwise, all chemicals used were purchased from Sigma-Aldrich, USA.

2D-PAGE. Protein concentration was estimated with a Bio-Rad *RC-DC* protein assay kit. For IEF, Bio-Rad 7 cm IPG strips were rehydrated with MSS containing the protein sample (200 μg to 300 μg) in a Bio-Rad Protean IEF Cell (50 V for 16 h) prior to focusing at 250 V for 15 min and 14,000 V-h (rapid ramping). The proteins in the IPG strip were equilibrated for 20 min with 6 M urea, 0.38 M Tris pH 8.8, 4% (w/v) SDS, 20% (v/v) glycerol and 2% (w/v) DTT and a further 20 min in the same buffer that consisted of 2.5% (w/v) iodoacetamide substituted for DTT. Equilibrated proteins were separated in a second dimension in manually cast 12%T SDS polyacrylamide gels. Gels were visualised via colloidal Coomassie G250 staining [34].

Gel image acquisition and densitometry analysis. Gel images were captured using the ProXPRESS scanner (Perkin Elmer). Spot detection and gel analyses were performed with the ProGENESIS Workstation 2005 software (Linear Dynamics) under default settings. Biological triplicate 2D gels were used to create average gels of SN15 and *gna1-35* for comparisons. Protein spots were considered differentially abundant if $p<0.05$ (unpaired t-test) and $\geq$two-fold difference in the normalised densitometry value of matching spots between the average gels (Supplementary Data 1). These spots were excised from gels and the proteins trypsin digested [35].

LC-MS/MS analysis and database searching. Tryptic digested peptides were analysed on an Agilent 1100 series capillary LC system coupled to an Applied Biosystems QSTAR Pulsar *i* LC-MS/MS system equipped with the IonSpray source in positive ion mode [35].

Mass spectra searches were performed with the Mascot search engine version 2.1.04 (Matrix Science) against the Broad-predicted protein set derived from the genome of *S. nodorum* (16,597 sequences; 6,455,598 residues), utilising error tolerances of ± 1.2 for MS and ± 0.6 for MS/MS, 'Max Missed Cleavages' set to one, the 'Oxidation (M)' variable modification and peptide charge set at 2+ and 3+. Results were filtered using 'Standard scoring', 'Max. number of hits' set to 20, 'Significance threshold' at $p<0.05$ and 'Ions score cut-off' at 15. Protein matches were considered positive with identifications that contained at least four matching peptides and MoWSE scores >100. A putative function was assigned to the matched protein by a BlastP homology search of the NCBI non-redundant protein database (minimum expected value cut-off score of 10^{-8}).

RNA isolation and RT-PCR. RNA isolation and gene transcript abundance was analysed essentially as previously described [36]. SN15 genomic DNA, prepared with a Retsch MM301 autolyser and Qiagen BioSprint 15, was used as a quantitative standard. Intron-spanning primers (Actin F/R) designed to amplify actin (*Act1*; EAT90788) were used to check all cDNA samples were free of genomic DNA via PCR (data not shown). All primer sequences from this study can be found in Supplementary Data 2

Gene expression analyses were performed using *in vitro*-grown fungal tissue and infected wheat leaves. *In vitro* gene expression analysis of SN15 and *gna1-35* was performed from transcripts extracted under the same growth conditions used for the 2D-PAGE analysis. Gene expression was normalised against *Act1* transcript abundance. Ef1α is more strongly expressed than *Act1* and was easier to detect on infected wheat leaves where fungal mRNA are limiting, particularly during early infection. Consequently, EF1α was used as the housekeeping gene for the *in planta* expression studies.

Gene expression between SN15 and *gna1-35* were deemed differentially abundant under the criteria that $p<0.05$ in an unpaired t-test and $\geq$two-fold difference in the normalised

transcript abundance. The expression of putative signalling target genes during SN15 infection on wheat was analysed with ANOVA set for Tukey-Kramer test in conjunction with a Dunnett's control. Gene expression was deemed significantly different if $p<0.05$ and $\geq$two-fold difference in the normalised transcript abundance relative to the Dunnett's control.

Construction of the *Sch1* gene knockout vector. *Sch1* was deleted by gene replacement with a phleomycin resistant selectable marker construct as previously described [32]. The 5' and 3' untranslated region (UTR) of *Sch1* was PCR amplified with the primer pairs 5'FwdXhoI-R567/5'RevHindIII-R567 and 3'FwdPstI-R567/3'RevNotI-R567, respectively. Restriction sites were introduced into the primer sequences to facilitate cloning with the phleomycin selectable marker plasmid vector pBSK-phleo [32]. The 5' *Sch1* UTR amplicon (562 bp) was cloned into *Xho*I and *Hin*dIII sites of pBSK-phleo to give pBSK-phleo-5'Sch1. The 3' *Sch1* UTR amplicon (850 bp) was cloned into *Pst*I and *Not*I sites of pBSK-phleo-5'Sch1 to give the knockout vector pBSK-Sch1KO. A 3.52 kb gene deletion KO construct was PCR-amplified from pBSK-Sch1KO using the primer pair R567FwdKO and R567RevKO primers.

Construction of the *Sch1* promoter-enhanced green fluorescent protein gene (eGFP) expression construct. The tissue expression pattern of *Sch1* was examined with transcriptional fusion of the putative *Sch1* promoter sequence and an eGFP gene. A 1.8 kb 5' UTR of *Sch1* containing two putative 'TATA' Goldberg-Hogness box core promoter sites [37, 38] was PCR-amplified with Sch1GFPtransF and Sch1GFPtransR. A partial fragment of pGPD-GFP [39] that consisted of eGFP, hygromycin resistance cassette and a *TrpC* terminator was also amplified with GFP-PCRf and GFP-PCRr. Both PCR fragments were fused using the Sch1GFPtransF and GFP-PCRr primers via overlapping PCR [32] with the resulting amplicon used for the subsequent transformation of SN15. PCR was used to test transformants for appropriate ectopic insertions.

Transformation of *S. nodorum*. The protocol for generating protoplasts and genetic transformation of *S. nodorum* SN15 was as previously described [7].

Southern analysis. The PCR amplicon of the primer pair 5'FwdXhoI-R567 and 5'FwdXhoI-R567 was used for random labelling to develop a probe for Southern analysis. This was performed as described elsewhere [7].

Infection assays. Detached leaf and whole plant spray assays were performed as described by Solomon et al. [40].

Histological techniques. Tissues for longitudinal-section histological examination were fixed and degassed overnight in formal acetic alcohol solution in glass vials [41]. For embedding in paraffin, tissues were dehydrated in an ascending series of ethanol (70%, 90% and 100% ethanol, 3 h for each step), then cleared in chloroform prior to infiltration with molten paraffin wax (Paraplast). The embedded tissues were sectioned at 10 μm using Shandon MX 35 knives on a Leica RM2235 microtome.

For embedding in Spurr's resin, the fixed tissues were washed in several changes of 0.025 M phosphate buffer and dehydrated in an ascending series of acetone (30%, 50%, 70%, 90% and 100% acetone, two changes of each solution and 15 min for each change). The tissues were then infiltrated with an ascending series of Spurr's resin (5% to 90%) [42] and then transferred to 100% Spurr's resin for 2 h, and again for overnight at room temperature before being polymerised at 60^{o}C. The embedded tissues were sectioned at 1 μm on a Reichert-Jung 2050 microtome.

The dsDNA specific stain dsDNA-specific 4',6-diamidino-2-phenylindole dilactate (DAPI) was used to stain paraffin tissue sections according to the manufacturer (Invitrogen). A mixture of 1% methylene blue and 1% azur II in 1% sodium tetraborate solution was used as a general stain as described elsewhere [43].

For transmission electron microscope (TEM) analysis, tissues embedded in Spurr's resin was sectioned at 80 nm using a diamond knife on a Reichart Ultracut E ultra-microtome. The sections were mounted onto 200 mesh copper grids (ProSciTech), stained for 20 min in a saturated aqueous solution of uranyl acetate, washed twice in distilled water, then stained in lead citrate for 4 min and washed again with several changes of distilled water [44]. The stained sections were examined at 80 kV on a Phillips CM100 Biotransmission EM.

For eGFP analysis, mycelia containing pycnidia of the *Sch1-eGFP* transformant grown on CzV8CS agar were excised and longitudinally handsliced with a double edge SS razor blade. Sections were viewed under differential interference contrast (DIC) and blue light excitation (460 to 490 nm) for eGFP fluorescence. Composite images were constructed with the DPManager software (Olympus).

Genbank accession numbers. Broad-annotated genes analysed in this study are available in the Genbank/EMBL databases under the accession numbers; EAT82552 (*Sch1*/SNOG_10217), EAT85007 (SNOG_07541), EAT85070 (SNOG_07604), EAT79369 (SNOG_13042), EAT81580 (SNOG_11081), EAT81149 (SNOG_11441) and EAT84551 (SNOG_08275).

RESULTS

Comparative proteomic analysis and the identification of genes that correspond to the differentially abundant proteins. The intracellular proteomes of SN15 and *gna1-35* were separated by 2D-PAGE (Fig. 1A and B). A total of 475 unique protein spots were identified in the SN15 and *gna1-35* samples. Of these, six spots were identified as being greater than two-fold different in abundance ($p<0.05$). Five spots (C1 to C5) were significantly less abundant and one spot (C6) showed an increase in abundance in *gna1-35*. LC-MS/MS was used to obtain spectra of peptides derived from these protein spots and the resulting data were matched against the *S. nodorum* predicted protein set to find the matching genes (Table 2). Seven genes were identified from the six differentially abundant protein spots. Proteins identified from spot C1 to C5 matched to genes that codes for a putative Concanamycin-induced protein C (*CipC*: SNOG_11081), a glutathione S-transferase (SNOG_07604), short-chain dehydrogenases (SNOG_10217 and SNOG_13042) and a proteasome subunit (SNOG_07541). Two proteins (C6-1 and C6-2) were identified from spot C6 and matched to genes that code for 3-dehydroquinate dehydratase (SNOG_11441) and a protein of unknown function (SNOG_08275).

Transcriptional analysis of putative heterotrimeric G protein signalling target genes. The expression of genes encoding putative heterotrimeric G protein signalling target proteins was examined with RT-PCR. This was performed to determine whether protein abundance was regulated at the transcriptional or post-transcriptional level. The normalised expression of each gene was compared with protein abundance data to identify relative correlations of protein and transcript abundances. Of the seven genes examined, four showed a positive correlation between protein and transcript abundance implying these genes are regulated at the transcriptional level (Fig. 2). Three of these genes showed transcriptional down regulation

(SNOG_13042, SNOG_10217 and SNOG_11081) whereas one (SNOG_11441) was up regulated in *gna1-35*. The other three genes showed no correlation between protein and transcript abundances (SNOG_07541, SNOG_07604 and SNOG_08275).

Quantitative RT-PCR was also used to determine the expression profile of these genes in *S. nodorum* during infection on wheat. Sampling time points were one, three, five and eight days post infection which coincided with host penetration, proliferation, onset and late pycnidiation, respectively [45]. Six of the genes identified from the proteomic analysis showed significantly differential expression during infection of detached wheat leaves by *S. nodorum* (Fig. 2). Five of these (SNOG_07541, SNOG_07604, SNOG_10217, SNOG_11441 and SNOG_13042) showed increased expression during late infection coinciding with asexual sporulation. One gene (SNOG_11081) was significantly more expressed during germination and penetration of the host at one day post infection. No expression was detected for SNOG_08275 during *in planta* growth.

SNOG_10217 encodes a putative short-chain dehydrogenase. The focus of this study was to identify and functionally characterise targets of Gna1-dependent regulation. SNOG_10217 was chosen for further analysis based on its strong down-regulation in the *gna1* strains. The open reading frame of SNOG_10217 consists of two introns and encodes a polypeptide of 299 amino acids with a predicted molecular mass (MM) and pI of 31.8 kDa and 5.5 respectively. These predicted figures closely match the experimental MM and pI as described above. SNOG_10217 contained a Pfam domain of the short-chain dehydrogenase family, thus the gene was subsequently named *Sch1*. Sch1 also possesses signature short-chain dehydrogenase motifs with inferred function in co-enzyme binding (T-G-V-S-G-G-I-G; residue 44 to 51) and structural stabilisation sequences (N-N-A-G; residue 125 to 128) [46]. BlastP [47] analysis of Sch1 revealed significant matches to hypothetical fungal short-chain dehydrogenases (40% to 50% amino acid identities).

***Sch1* is highly expressed in pycnidia**. Examination of gene expression by quantitative PCR showed that *Sch1* transcript abundance was maximal during the latter stages of infection implying a role for Sch1 in asexual sporulation. To gain a more detailed understanding of expression during asexual development, a transcriptional fusion consisting of the *Sch1* 5' putative promoter region fused to the eGFP gene was constructed and transformed into SN15. Subsequent transformants were screened with those demonstrating comparable phenotype and pathogenicity to wild-type *S. nodorum* chosen for further analysis (data not shown). eGFP expression was examined *in vitro* by excising hyphae and pycnidia from the transformed strain growing on complex CzV8CS agar (Fig. 3). Images collected from DIC microscopy showed asexual sporulation occurring at varying stages of development on the agar. Examination of these samples for eGFP expression highlighted that fluorescence was localised strictly to within mature pycnidia or differentiating asexual structures, known as mycelial knots. Fluorescence was not observed in vegetative mycelia. Higher magnification data revealed eGFP expression was observed in the pycnidial cavity that consisted of the sub-parietal tissue layer and asexual pycnidiospores but not the melanised pycnidial wall. These results confirm the strong expression of *Sch1* during asexual development and demonstrate the specificity of the expression in the sporulation structures.

Targeted gene deletion of *Sch1*. The eGFP expression analysis highlighted a potential role for Sch1 in asexual development. Mutants of *S. nodorum* lacking *Sch1* were created by homologous recombination with a *Sch1* gene deletion construct conferring phleomycin resistance (Fig. 4A). Initial PCR screening enabled the recovery of two independently derived gene deletion mutants designated as *S. nodorum sch1-11* and *sch1-42* and an ectopic strain designated as *Sch1-30*. Southern analysis confirmed the presence of *Sch1* in *Sch1-30* and successful gene deletion in *sch1-11* and *sch1-42* (Fig. 4B). 2D-PAGE of the transformants confirmed that the protein spot corresponding to Sch1 was present in SN15 and *Sch1-30* but

not in the *sch1* mutants (Fig. 4C). This indicates a correct protein-to-gene assignment via mass spectrometry identification and unequivocal evidence of gene deletion.

***Sch1* deletion affects vegetative growth**. Vegetative growth of the *sch1* strains was compared with SN15 and *Sch1-30* on solid agar media. All strains examined demonstrated a similar radial growth rate on complex CzV8CS agar with the *sch1* mutants producing a green pigment in older mycelia (Fig. 5A). When grown on defined minimal medium (MM) agar, the *sch1* mutants showed a significant reduction in radial growth compared to both SN15 and *Sch1-30*. The inclusion of components from the complex media into the MM failed to complement the growth defect implying the phenotype is more than a simple auxotrophic response. The vegetative phenotype of the *sch1* mutants was also investigated when grown as submerged cultures in shaking flasks consisting of MM broth. At 24 hours post inoculation, the mycelia of both SN15 and the ectopic mutant was dispersed throughout the media as is typically observed. The mycelia of the *sch1* strains were not dispersed but appeared to aggregate into a single mass (data not shown).

Based on the phenotypic variation apparent from these simple *in vitro* growth assays, we attempted to complement the mutation by re-introducing the *Sch1* gene into the *sch1* background. Attempts to generate the required number of *sch1* protoplasts proved difficult, most likely due to the clumping phenotype observed in the shaking flasks. Multiple flasks were attempted to generate sufficient protoplasts but this too was unsuccessful. Consequently, genetic complementation of the *sch1* strains was not possible.

***Sch1* is dispensable for proliferation on wheat.** The *sch1* mutants were examined for their ability to cause lesions on wheat. A detached leaf assay was used to measure the progress of lesion development from a single point inoculation over a 14 day period. Lesion sizes caused by all fungal strains on detached wheat leaves were not significantly differently (data not shown). A whole plant spray assay was also used to simulate a field infection by

spraying spore suspensions onto two week old wheat plants. The disease scores for all strains were comparable indicating that *Sch1* is dispensable for lesion development on wheat (data not shown).

Sch1* deletion affects asexual sporulation *in vitro* and *in planta. The eGFP-fusion experiments revealed the localised nature of *Sch1* expression during asexual development. Also apparent from the sub-culturing and harvesting of the *sch1* strains was the very low numbers of spores recovered. To analyse the sporulation phenotype further, pycnidiospores of all strains were harvested and compared via light microscopy (Fig. 5B). Spore suspensions derived from SN15 and *Sch1-30* were predominantly composed of pycnidiospores. The spore suspensions harvested from the *sch1* strains contained far fewer spores and much of what was assumed to be mycelial debris. Quantitative analysis of the spores harvested showed an approximate 50-fold decrease in the number produced by the *sch1* strains (Fig. 6C). Significantly fewer pycnidiospores were also produced by the *sch1* strains *in planta* implying the phenotype is not restricted to a specific growth environment (Fig. 6D). The *sch1* deletion also resulted in reduced average spore length (Fig. 6E) although the germination rate of the mutants was unaffected (data not shown).

Sch1* is required for pycnidial development *in vitro* and *in planta. Abnormalities in asexual sporulation of the *sch1* mutants prompted further studies of the mutant pycnidia. The pycnidia of SN15 and *Sch1-30* exuded a pink cirrhi when grown on CZV8Cs, whilst the cirrhi secreted by the *sch1* pycnidia appeared much paler, almost white, and less abundant (Fig. 6A). On wheat leaves, the mutant phenotype was further exaggerated with the *sch1* strains not exuding visible cirrhi from the pycnidia (Fig. 6B). The diameter of *sch1* pycnidia was also significantly smaller than those of the wild-type or ectopic both *in vitro* and *in planta* suggesting a structural role for Sch1 (Fig. 6C and D).

The ontogeny of SN15 and *sch1-42* pycnidia *in vitro* was compared via tissue longitudinal-sectioning and visualisation with DIC, bright field (BF) and transmission electron microscopy (Fig. 7A). Immediately apparent was the smaller size of the *sch1* pycnidium confirming the measurements reported above. Within the pycnidial cavity, far few pycnidiospores were present for the mutant which is consistent with the much lower density of spores demonstrated in the exuding cirrhus. The cell walls of the two strains were also structurally different with the cells within the SN15 wall appearing more uniform than the corresponding cells in *sch1-42*.

The pycnidia of *sch1-42* showed similar developmental defects during growth on wheat leaves (Fig. 7B). The contents of the pycnidial cavity again significantly differed with the wildtype cavity comprising of tightly packed uniform spores. Surrounding the cavity is the sub-parietal layer that lines the inner wall of the pycnidium. The sub-parietal layer was evident in SN15 as a dense ring enveloping the cavity but was poorly defined for the *sch1* strain. It was further observed that the conidiogenous cells in *sch1-42* were unable to differentiate into distinct pycnidiospores. As witnessed for the *in vitro* samples, the pycnidial wall cells of SN15 and *sch1-42* were morphologically different as indicated by the staining pattern.

TEM was used to interpret the structural alteration of *sch1* pycnidia in greater detail (Fig. 7Biii and vi). It was observed that a substantial portion of most SN15 pycnidial wall cells was occupied by a vacuole. Electron dense materials, presumed to be cytoplasmic constituents, were often located adjacent to the intracellular side of the cell wall. In contrast, corresponding cells in *sch1-42* contained multiple small vacuoles and a high proportion of cytoplasmic constituents.

It was observed that the pycnidia of *sch1-42* resembled previously described immature pycnidia of *S. nodorum* [48]. Hence, it was possible that Sch1 may be involved in the

differentiation of the pycnidial primordium to maturity. To test this hypothesis, SN15 (mature and developing) and *sch1-42* pycnidia were examined for nuclei distribution using DAPI staining (Fig. 8). The mature SN15 sub-parietal layer was distinguishable from the cell wall as the latter tissue revealed comparatively less nuclei. Nuclei were also observed in spores located in the pycnidial cavity amidst the background fluorescence. The pycnidial cell wall and sub-parietal layer of *sch1-42* were indistinguishable as the DAPI staining indicated that most cells surrounding the pycnidial cavity were nucleated. DAPI staining of an immature pycnidium of SN15 showed a similar nuclei distribution pattern to *sch1-42* (Fig. 8). Collectively, these data suggest that the pycnidial wall of *sch1-42* may be attenuated in pycnidial maturation.

Sch1 regulation is independent of Ca2+/calmodulin signalling. Sch1 abundance was examined in previously characterised signalling mutant strains lacking the MAP kinase *Mak2* and the Ca^{2+}/calmodulin protein kinase *CpkA* [32, 49]. The level of Sch1 protein in the *cpkA* strain was not significantly different from SN15 suggesting that the regulation of Sch1 is independent of the Ca^{2+}/calmodulin-dependent signalling (Fig. 9). The amount of Sch1 protein was significantly less in the *mak2* strain than in SN15 but was comparable to the level observed in *sch1-42* suggesting that the Mak2 MAP kinase signalling pathway has a role in the regulation of Sch1.

DISCUSSION

We have previously shown that inactivation of Gna1 has resulted in extensive changes in the phenotype and pathogenicity *S. nodorum*. Hence, the aim of this study was to identify and functionally characterise proteins in the pathogen *S. nodorum* that are regulated by signalling events associated with the Gα subunit Gna1.

2D-PAGE was used to directly compare the intracellular proteomes of the *gna1* and wildtype *S. nodorum*. The analysis of the 2D-PAGE dataset led to the identification of seven intracellular proteins that were regulated at a significant level by Gna1 in biological independent samples analysed in triplicate. The subsequent data were subjected to rigorous statistical analysis with only proteins with significant differences reported. A less stringent approach would have resulted in the identification of many more 'regulated' proteins, but their biological significance would have been questionable.

The seven genes identified encode for putative proteins of diverse function. SNOG_11081 encodes a putative Concanamycin induced protein C. CipC was first identified as an accumulated protein in *Aspergillus nidulans* exposed to the antibiotic concanamycin A [50]. Orthologs of *CipC* were also identified in other fungi however their function is unknown [24, 51-54]. The gene expression profile of *CipC in planta* showed maximal transcript abundance during one day post infection which suggests that this gene may play a role during early infection. Gene disruption of SNOG_11081 had no effect on pathogenicity or phenotype of *S. nodorum* (data not shown). SNOG_07694 and SNOG_13042 encode a putative glutathione S-transferase and short-chain dehydrogenase respectively. These too were subsequently characterised by gene disruption. The resulting mutants appeared identical to the wild-type strain implying that these genes, whilst regulated by *Gna1*, did not significantly contribute to the phenotype of the *gna1* strains (data not shown).

The disruption of a fourth gene, SNOG_10217, generated strains of *S. nodorum* unable to differentiate mature pycnidia. Sequence analysis of SNOG_10217 identified it as also belonging to the family of short-chain dehydrogenase and the gene was subsequently named *Sch1*. The pycnidia developed by *sch1* strains were smaller and contained a significantly lower number of pynidiospores which appeared abnormal in shape. Histological analysis of these mutant pycnidia highlighted significant structural differences compared to wild-type including the spore density and shape within the pycnidial cavity and also structural deformity of the sub-parietal layer and pycnidial wall.

It was observed that the protein sequences of Sch1 and SNOG_13042 shared approximately 30% similarity. On this basis, we investigated whether SNOG_13042 was partially compensating for the loss of Sch1 in the sch1 strains via the creation of a double mutant lacking both Sch1 and Sch2. The resulting mutants were identical to the sch1 strains strongly suggesting that Sch2 is not compensating for the loss of Sch1 (Supplementary Data 3).

There have been several recent reports examining the molecular and biochemical requirements of asexual sporulation in *S. nodorum*. The cAMP-dependent (*Gna1*), MAP kinase (*Mak2*) and calcium signalling pathways (*CpkA*) all have a demonstrated role in sporulation [7, 32, 33]. Analyses in this study have shown that Sch1 is regulated by *Gna1* and *Mak2* but not *CpkA*. Shared regulation by the cAMP-dependent and MAP-kinase signalling pathways was not unexpected as cross-talk between these pathways has been well documented [55, 56].

The presence of the sugar alcohol mannitol has also been identified as a requirement for *S. nodorum* to undergo asexual sporulation [40, 57, 58]. The levels of mannitol appear unchanged when comparing the *sch1* strains with SN15; excluding it as having a role in the

sch1 defect (data not shown). Hence, *Sch1* appears to be a novel factor in *S. nodorum* required for appropriate sporulation.

Douaiher et al (2004) have previously reported the ontogeny of *S. nodorum* pycnidia *in vitro*. This detailed examination elegantly described the differentiation of a pycnidium from the initial formation of the mycelial knot through to a fully mature structure. A comparative analysis of these structures described by Douaiher et al with those produced by the *sch1* strains indicate that differentiation of the *sch1* pycnidia is interrupted through the development of the pynidial primordium. This stage has been defined as the formation and the extension of the pycnidial cavity and conidiogenesis. A pycnidial cavity has clearly formed for the *sch1* structures but the conidiogenesis cells are difficult to distinguish. Furthermore, using DAPI staining we have shown that the walls of *sch1-42* pycnidia contain a similar nuclei distribution to that of an immature pycnidium of SN15. Hence, the evidence reported here indicates that the *Sch1* gene/product has a discrete role in this stage of pycnidial development

Many important phytopathogenic fungi such as *Cryphonectria parasitica*, *Cochliobolus heterostrophus* and *Mycosphaerella graminicola* are capable of asexual sporulation through pycnidia. Recent studies have identified various signalling pathways as having a role in pycnidial development in these fungi [59, 60]. Similar studies in *S. nodorum* also identified that the calcium/calmodulin-dependent protein kinase CpkA was required for proper pycnidial differentiation [32]. However the genes and proteins regulated by these signalling pathways that are required for development of wild-type pycnidia are yet to be identified. To our knowledge, *Sch1* is the first signal transduction target identified to play a required role in the development of pycnidia.

Three additional genes were identified during the course of this study as regulated by G protein signalling, but are yet to be functionally characterised. SNOG_07541 encodes an

alpha type 2 proteasome subunit which comprises part of the 20S proteasome, the central enzyme of nonlysosomal protein degradation in both the cytosol and nucleus [61]. SNOG_08275 encodes a protein of unknown function that is not expressed during infection, while SNOG_11441 enocodes a putative dehydroquinate dehydratase. The 3-dehydroquinate dehydratase protein is associated with quinate metabolism [62]. In *Neurospora crassa*, Qa-2p is required for the conversion of 3-dehydroquinate to 3-dehydroshikimate. Both compounds are intermediates of aromatic amino acid biosynthesis and quinate catabolism pathways [62, 63]. It is possible that the increased abundance of the Qa-2p orthologue in *S. nodorum* may have led to a perturbation of the aromatic amino acid pathway. This in turn may have affected dihydroxyphenylalanine melanin biosynthesis in the *gna1* strains and resulting in the albino vegetative phenotype previously reported. However, this hypothesis requires further investigation.

A thorough gene expression analysis, both *in vitro* and *in planta*, was undertaken on the genes encoding the seven proteins. Quantitative transcript measurements revealed a correlation between protein and transcript abundance in four of the seven genes. Three of the genes were down-regulated in the *gna1* background whilst one was up-regulated. The protein and transcript abundance in the three remaining genes did not correlate *in vitro*. Similar observations were previously made from studies of other biological systems using both proteomics and transcriptomics to analyse gene expression [64, 65]. This may be attributed to post-transcriptional regulation or differing half-lives of transcripts and proteins [66, 67]. Nevertheless, some of these genes showed a differential expression pattern during infection suggestive of transcriptional regulation by unknown factors.

This study has demonstrated that 2D-PAGE is an effective method for analysing the proteomes for downstream targets of signalling pathways that are differentially accumulated between *S. nodorum* SN15 and *gna1* strains. The genes encoding several of these proteins

were functionally characterised by gene disruption. Through this approach, the short-chain dehydrogenase *Sch1*, which is subjected to positive regulation by Gna1, was found to be required for the differentiation of pycnidia. *S. nodorum* is a polycyclic pathogen, and as such, asexual sporulation is an attractive target for investigating mechanisms of disease control. It is relevant to note that although deformed, the *sch1* strains were able to form pycnidia. In contrast, the *Gna1* mutants were unable to differentiate pycnidia suggesting that additional unidentified signalling targets are required to initiate pycnidial formation from precursor hyphal cells. It should also be considered that proteome changes observed in this study may have been the result of perturbation in other parts of the heterotrimeric G protein pathway rather than Gna1 alone. Therefore, the proteins identified could have been directly or indirectly regulated by Gna1.

We anticipate that this study will stimulate research to further understand the biology of pycnidial development in other fungal pathogens and its requirement for the establishment of diseases.

ACKNOWLEDGEMENTS

We thank Kasia Rybak for technical assistance and Dr. Barbara J. Howlett at The University of Melbourne for providing the pGPD-GFP construct. This research was supported by the Grains Research and Development Corporation. K.-C.T. was funded by an Australian Postgraduate Award. JLH and AHM were supported as an ARC Australian Post-doctoral Fellow and an ARC Australian Professorial Fellow, respectively.

REFERENCES

1. Simon, M.I., M.P. Strathmann, and N. Gautam, *Diversity of G proteins in signal transduction.* Science, 1991. **252**(5007): p. 802-8.
2. Borkovich, K.A., *Signal transduction pathways and heterotrimeric G proteins*, in *The Mycota*, R. Brambl and G.A. Marzluf, Editors. 1996, Springer-Verlag: Berlin.
3. Neves, S.R., P.T. Ram, and R. Iyengar, *G protein pathways.* Science, 2002. **296**(5573): p. 1636-9.
4. Kurose, H., *$G\alpha_{12}$ and $G\alpha_{13}$ as key regulatory mediator in signal transduction.* Life Sci, 2003. **74**(2-3): p. 155-61.
5. Bolker, M., *Sex and crime: heterotrimeric G proteins in fungal mating and pathogenesis.* Fungal Genet Biol, 1998. **25**(3): p. 143-56.
6. Lee, N., C.A. D'Souza, and J.W. Kronstad, *Of smuts, blasts, mildews, and blights: cAMP signaling in phytopathogenic fungi.* Annu Rev Phytopathol, 2003. **41**: p. 399-427.
7. Solomon, P.S., et al., *The disruption of a $G\alpha$ subunit sheds new light on the pathogenicity of Stagonospora nodorum on wheat.* Mol Plant-Microbe Interact, 2004. **17**(5): p. 456-66.
8. Yamagishi, D., H. Otani, and M. Kodama, *G protein signaling mediates developmental processes and pathogenesis of Alternaria alternata.* Mol Plant-Microbe Interact, 2006. **19**(11): p. 1280-8.
9. Gronover, C.S., et al., *The role of G protein α subunits in the infection process of the gray mold fungus Botrytis cinerea.* Mol Plant-Microbe Interact, 2001. **14**(11): p. 1293-302.

10. Horwitz, B.A., et al., *A G protein α subunit from Cochliobolus heterostrophus involved in mating and appressorium formation.* Fungal Genet Biol, 1999. **26**(1): p. 19-32.
11. Gao, S. and D.L. Nuss, *Distinct roles for two G protein α subunits in fungal virulence, morphology, and reproduction revealed by targeted gene disruption.* Proc Natl Acad Sci USA, 1996. **93**(24): p. 14122-14127.
12. Jain, S., et al., *Targeted disruption of a G protein α subunit gene results in reduced pathogenicity in Fusarium oxysporum.* Curr Genet, 2002. **41**(6): p. 407-13.
13. Liu, S. and R.A. Dean, *G protein α subunit genes control growth, development, and pathogenicity of Magnaporthe grisea.* Mol Plant-Microbe Interact, 1997. **10**(9): p. 1075-86.
14. Liu, H., et al., *Rgs1 regulates multiple Gα subunits in Magnaporthe pathogenesis, asexual growth and thigmotropism.* EMBO J, 2007. **26**: p. 690-700.
15. Fang, E.G. and R.A. Dean, *Site-directed mutagenesis of the magB gene affects growth and development in Magnaporthe grisea.* Mol Plant-Microbe Interact, 2000. **13**(11): p. 1214-27.
16. Regenfelder, E., et al., *G proteins in Ustilago maydis: transmission of multiple signals?* EMBO J, 1997. **16**(8): p. 1934-42.
17. Gronover, C.S., C. Schorn, and B. Tudzynski, *Identification of Botrytis cinerea genes up-regulated during infection and controlled by the Gα subunit BCG1 using suppression subtractive hybridization (SSH).* Mol Plant-Microbe Interact, 2004. **17**(5): p. 537-46.
18. Siewers, V., et al., *Functional analysis of the cytochrome P450 monooxygenase gene bcbot1 of Botrytis cinerea indicates that botrydial is a strain-specific virulence factor.* Mol Plant-Microbe Interact, 2005. **18**(6): p. 602-12.

19. Dawe, A.L., et al., *Microarray analysis of Cryphonectria parasitica Gα- and Gβγ-signalling pathways reveals extensive modulation by hypovirus infection.* Microbiol, 2004. **150**(Pt 12): p. 4033-43.
20. Phalip, V., et al., *Diversity of the exoproteome of Fusarium graminearum grown on plant cell wall.* Curr Genet, 2005. **48**(6): p. 366-79.
21. Fernandez-Acero, F.J., et al., *Two-dimensional electrophoresis protein profile of the phytopathogenic fungus Botrytis cinerea.* Proteomics, 2006. **6**: p. S88-96.
22. Cooper, B., W.M. Garrett, and K.B. Campbell, *Shotgun identification of proteins from uredospores of the bean rust Uromyces appendiculatus.* Proteomics, 2006. **6**(8): p. 2477-84.
23. Paper, J.M., et al., *Comparative proteomics of extracellular proteins in vitro and in planta from the pathogenic fungus Fusarium graminearum.* Proteomics, 2007. **7**(17): p. 3171-83.
24. Bohmer, M., et al., *Proteomic analysis of dimorphic transition in the phytopathogenic fungus Ustilago maydis.* Proteomics, 2007. **7**(5): p. 675-85.
25. Rampitsch, C., et al., *Analysis of the wheat and Puccinia triticina (leaf rust) proteomes during a susceptible host-pathogen interaction.* Proteomics, 2006. **6**(6): p. 1897-907.
26. Kim, S.T., et al., *Proteome analysis of rice blast fungus (Magnaporthe grisea) proteome during appressorium formation.* Proteomics, 2004. **4**(11): p. 3579-87.
27. Dean, R.A., et al., *The genome sequence of the rice blast fungus Magnaporthe grisea.* Nature, 2005. **434**(7036): p. 980-6.
28. Kamper, J., et al., *Insights from the genome of the biotrophic fungal plant pathogen Ustilago maydis.* Nature, 2006. **444**(7115): p. 97-101.

29. Cuomo, C.A., et al., *The Fusarium graminearum genome reveals a link between localized polymorphism and pathogen specialization.* Science, 2007. **317**(5843): p. 1400-2.
30. Hane, J.K., et al., *Dothideomycete plant interactions illuminated by genome sequencing and EST analysis of the wheat pathogen Stagonospora nodorum.* Plant Cell, 2007. **19**(11): p. 3347-68.
31. Solomon, P.S., et al., *Stagonospora nodorum: cause of stagonospora nodorum blotch of wheat.* Mol. Plant Pathol., 2006. **7**(3): p. 147-156.
32. Solomon, P.S., et al., *Investigating the role of calcium/calmodulin-dependent protein signalling in Stagonospora nodorum.* Molecular Microbiology, 2006. **62**: p. 367-381.
33. Solomon, P.S., et al., *The Mak2 MAP kinase signal transduction pathway is required for pathogenicity in Stagonospora nodorum.* Curr Genet, 2005. **48**(1): p. 60-8.
34. Neuhoff, V., et al., *Improved staining of proteins in polyacrylamide gels including isoelectric focusing gels with clear background at nanogram sensitivity using Coomassie Brilliant Blue G-250 and R-250.* Electrophoresis, 1988. **9**(6): p. 255-62.
35. Taylor, N.L., et al., *Differential impact of environmental stresses on the pea mitochondrial proteome.* Mol Cell Proteomics, 2005. **4**(8): p. 1122-33.
36. Solomon, P.S., et al., *The utilisation of di/tripeptides by Stagonospora nodorum is dispensable for wheat infection.* Physiological and Molecular Plant Pathology, 2003. **63**(4): p. 191-199.
37. Lifton, R.P., et al., *The organization of the histone genes in Drosophila melanogaster: functional and evolutionary implications.* Cold Spring Harb Symp Quant Biol, 1978. **42**: p. 1047-51.
38. Smale, S.T. and J.T. Kadonaga, *The RNA polymerase II core promoter.* Annu Rev Biochem, 2003. **72**: p. 449-79.

39. Sexton, A.C. and B.J. Howlett, *Green fluorescent protein as a reporter in the Brassica-Leptosphaeria maculans interaction.* Physiological and Molecular Plant Pathology, 2001. **58**(1): p. 13-21.
40. Solomon, P.S., K.-C. Tan, and R.P. Oliver, *Mannitol 1-phosphate metabolism is required for sporulation in planta of the wheat pathogen Stagonospora nodorum.* Mol Plant-Microbe Interact, 2005. **18**(2): p. 110-5.
41. Sass, J.E., *Botanical Microtechnique*1958, Ames: Iowa State University Press.
42. Spurr, A.R., *A low-viscosity epoxy resin embedding medium for electron microscopy.* J Ultrastruct Res, 1969. **26**(1): p. 31-43.
43. Richardson, K.C., L. Jarret, and E.H. Finke, *Embedding in epoxy resins for ultrathin sectioning in electron microscopy.* Stain Tech., 1960. **35**: p. 313-323.
44. Venable, J.H. and R. Coggshall, *A simplified lead citrate stain for electron microscopy.* J. Cell Biol., 1965. **25**: p. 407-408.
45. Solomon, P.S., et al., *Structural characterisation of the interaction between Triticum aestivum and the dothideomycete pathogen Stagonospora nodorum.* Eur J Plant Pathol, 2006. **114**(3): p. 275-282.
46. Oppermann, U., et al., *Short-chain dehydrogenases/reductases (SDR): the 2002 update.* Chem Biol Interact, 2003. **143-144**: p. 247-53.
47. Altschul, S.F., et al., *Gapped BLAST and PSI-BLAST: a new generation of protein database search programs.* Nucleic Acids Res, 1997. **25**(17): p. 3389-402.
48. Douaiher, M.N., R. Halama, and M.C. Janex-Favre, *The ontogeny of Stagonospora nodorum pycnidia in culture.* Sydowia, 2004. **56**(1): p. 39-50.
49. Solomon, P.S., et al., *The Mak2 MAP kinase signal transduction pathway is required for pathogenicity in Stagonospora nodorum.* Current Genetics, 2005. **48**(1): p. 60-68.

50. Melin, P., J. Schnurer, and E.G. Wagner, *Proteome analysis of Aspergillus nidulans reveals proteins associated with the response to the antibiotic concanamycin A, produced by Streptomyces species.* Mol Genet Genomics, 2002. **267**(6): p. 695-702.
51. Le Quere, A., et al., *Divergence in gene expression related to variation in host specificity of an ectomycorrhizal fungus.* Mol Ecol, 2004. **13**(12): p. 3809-3819.
52. Morel, M., et al., *Identification of genes differentially expressed in extradical mycelium and ectomycorrhizal roots during Paxillus involutus-Betula pendula ectomycorrhizal symbiosis.* Appl Environ Microbiol, 2005. **71**(1): p. 383-391.
53. Peter, M., et al., *Analysis of expressed sequence tags from the ectomycorhizal basidiomycetes Lacarria bicolor and Pisolithus microcarpus.* New Phytol, 2003. **159**(1): p. 117-129.
54. Teichert, S., et al., *Deletion of the Gibberella fujikuroi glutamine synthetase gene has significant impact on transcriptional control of primary and secondary metabolism.* Mol Microbiol, 2004. **53**(6): p. 1661-75.
55. Nishimura, M., G. Park, and J.R. Xu, *The G-beta subunit MGB1 is involved in regulating multiple steps of infection-related morphogenesis in Magnaporthe grisea.* Molecular Microbiology, 2003. **50**(1): p. 231-243.
56. Kaffarnik, F., et al., *PKA and MAPK phosphorylation of Prf1 allows promoter discrimination in Ustilago maydis.* EMBO Journal, 2003. **22**(21): p. 5817-5826.
57. Solomon, P.S., et al., *Mannitol is required for asexual sporulation in the wheat pathogen Stagonospora nodorum (glume blotch).* Biochem J, 2006. **399**(2): p. 231-9.
58. Solomon, P.S., O.D.C. Waters, and R.P. Oliver, *Decoding the enigmatic mannitol in filamentous fungi.* Trends in Microbiology, 2007. **15**: p. 257-262.

59. Cousin, A., et al., *The MAP kinase-encoding gene MgFus3 of the non-appressorium phytopathogen Mycosphaerella graminicola is required for penetration and in vitro pycnidia formation.* Mol Plant Pathol, 2006. **7**(4): p. 269-278.
60. Mehrabi, R. and G.H.J. Kema, *Protein kinase a subunits of the ascomycete pathogen Mycosphaerella graminicola regulate asexual fructification, filamentation, melanization and osmosensing.* Molecular Plant Pathology, 2006. **7**(6): p. 565-577.
61. Marchler-Bauer, A., et al., *CDD: a curated Entrez database of conserved domain alignments.* Nucleic Acids Research, 2003. **31**: p. 383-387.
62. Giles, N.H., et al., *The Wilhelmine E. Key 1989 invitational lecture. Organization and regulation of the qa (quinic acid) genes in Neurospora crassa and other fungi.* J Hered, 1991. **82**(1): p. 1-7.
63. Harwood, C.S. and R.E. Parales, *The β-ketoadipate pathway and the biology of self-identity.* Annu Rev Microbiol, 1996. **50**: p. 553-90.
64. Fessler, M.B., et al., *A genomic and proteomic analysis of activation of the human neutrophil by lipopolysaccharide and its mediation by p38 mitogen-activated protein kinase.* J Biol Chem, 2002. **277**(35): p. 31291-302.
65. Gygi, S.P., et al., *Correlation between protein and mRNA abundance in yeast.* Mol Cell Biol, 1999. **19**(3): p. 1720-30.
66. Kozak, M., *Regulation of translation via mRNA structure in prokaryotes and eukaryotes.* Gene, 2005. **361**: p. 13-37.
67. Mann, M. and O.N. Jensen, *Proteomic analysis of post-translational modifications.* Nat Biotechnol, 2003. **21**(3): p. 255-61.

FIGURE LEGENDS

Figure 1. (A) Representative 2D-PAGE gels of SN15 and *gna1-35* showing differentially abundant proteins in the intracellular proteomes. (B) Sub-panels of the regions marked in (A) for each of the biological triplicate samples. Gels representing each of the biological triplicates are available in Supplementary Data 4.

Figure 2. Protein/transcript abundance graphs for each of the targets identified via 2D-PAGE. The transcript profiling of each gene is comprised of two panels. The panel on the left is a comparison of relative protein (white bars) and transcript (black bars) levels for each of the targets *in vitro*. Asterisks located on top of bar graphs signify significant differences in protein and transcript abundances. 'S' and 'G' on the *x*-axis denote SN15 and *gna1-35*, respectively. The panels on the right (line graphs) depict gene expression *in planta* for each target gene. Numbers on the *x*-axis are days post infection and * denotes differential gene expression relative to the Dunnett's control group 'D'. The y-axis represents relative gene expression normalised to actin (*in vitro*) of EF1α (*in planta*). SE bars are shown.

Figure 3. Expression of the *Sch1* promoter-eGFP fusion construct in SN15. Longitudinal section images taken with DIC microscopy showing hyphae, mature and immature pycnidia (mycelial knots). (A), (B) and (C) represent increasing magnification. C, conidiogenous cell; Cv, pycnidial cavity; H, hyphae; MK, mycelial knot; P, pycnidium; S, spore; SL, sub-parietal layer and W, pycnidial wall.

Figure 4. Construction of the *sch1* mutants. (A) (i) The *Sch1* knockout vector was constructed by ligating PCR amplified 5' and 3' untranslated region (UTR) of *Sch1* to the

*Xho*I/*Hin*dIII and *PstI*/*Not*I restriction sites of pBSK-phleo, respectively. (ii) The knockout vector was PCR-amplified and transformed into SN15 to facilitate (iii) homologous gene replacement. Restriction sites are as follows, X. *Xho*I; H. *Hin*dIII; P. *Pst*I and N. *Not*I. Primers are as follows; *1.* 5'FwdXhoI-R567, *2.* 5'RevHindIII-R567, *3.* 3'FwdPstI-R567, *4.* 3'RevNotI-R567, *5.* R567FwdKO and *6.* R567RevKO. Primer sequences are listed in Supplemental Table 2 online. Probe used for Southern analysis is indicated. (B) Southern analysis of *S. nodorum* SN15 (i), *Sch1-30* (ii), *sch1-11* (iii) and *sch1-42* (iv). Bands corresponding to 4.2 and 5.5 kb were predicted for strains carrying an intact and deleted gene, respectively. Genomic DNA was digested with *Xho*I prior to blotting. (C) Detection of Sch1 via 2D-PAGE (arrows).

Figure 5. Vegetative morphology of the *sch1* mutants. (A) Colony morphology after two weeks growth on CzV8CS and MM agar. (B) Light microscope images of pycnidiospores (arrows) harvested from *S. nodorum* SN15, *Sch1-30*, *sch1-11* and *sch1-42*. Notice the mycelial debris associated with the spores of the *sch1* mutants. (C) Spores per plate from strains grown on CzV8CS agar for two weeks. Mean values were calculated from three spore counts of biological pooled plate replicates of SN15 (n = 3), *Sch1-30* (n = 3), *sch1-11* (n = 11) and *sch1-42* (n = 12). (D) *In planta* sporulation assay. Mean values were calculated from three spore counts of pooled spores derived from biological infected replicates; SN15 (n = 10), *Sch1-30* (n = 10), *sch1-11* (n = 5) and *sch1-42* (n = 5). (E) A comparison of the average spore length of SN15, *Sch1-30* and *sch1-42* (n = 34). Note that an asterisk denotes a significant difference to SN15 ($p<0.05$).

Figure 6. *Sch1* deletion affects pycnidial function and size. (A) Digital images of pycnidia produced on CzV8CS agar and (B) wheat leaves. Pycnidia of the *sch1* mutants rarely exude

spores. Key = Ch, cirrhus and Py, pycnidium. (C) The average diameter of pycnidia derived from growth on CzV8CS agar (SN15, n = 191; Sch1-30, n = 146; *sch1-11*, n = 144 and *sch1-42*, n = 286) and (D) wheat leaves (SN15, n = 69; Sch1-30, n = 69; *sch1-11*, n = 151 and *sch1-42*, n = 184). Note that an asterisk denotes a significant difference to SN15 ($p<0.05$).

Figure 7. Analysis of SN15 and *sch1-42* pycnidia via longitudinal sectioning. **(A)** The morphology SN15 and *sch1-42* melanised pycnidial wall (i and iii) and cirrhi (ii and iv) are demonstrated via paraffin embedding and sectioning. Magnified images of the unstained pycnidial wall cellular arrangements (v and vii) and cirrhi (vi and viii) are shown. **(B)** Spurr's resin embedding sectioning of SN15 (i, ii and iii) and *sch1-42* (iv, v and vi) pycnidia showing greater details of cells of the pycnidial wall and the sub-parietal layer. (i) and (iv) show pycnidia of SN15 and *sch1-42*. (ii) and (v) are images taken from increase magnifications of the pycnidial wall and cavity interface of SN15 and *sch1-42* pycnidia. Cells of the pycnidia wall were examined via TEM (iii and vi). C; conidiogenous cell; Ch, cirrhus; Cp, cytoplasm; Cv, pycnidial cavity; N, nucleus; PC; plant cell; Py, pycnidium; OC, ostiolar cone; S, spore; SL; sub-parietal layer; Vc, vacuole and W, pycnidial wall.

Figure 8. The nuclear content of SN15 and *sch1-42* pycnidia was examined from longitudinal tissue sections stained with DAPI. (A) A comparison of nuclei distribution in pycnidia of SN15 at different stages of development and *sch1-42*. Boxes are expanded in (B) showing greater magnification of DAPI-stained cell wall and sub-parietal layer regions of SN15 and *sch1-42* pycnidia. Key; Cv, pycnidial cavity; N, nucleus; OC, ostiolar cone; SL; sub-parietal layer; Vc, vacuole and W, pycnidial wall [prefix (D), developing; (M), mature.

1 Figure 9. Representative regions of 2D gels from *S. nodorum* SN15, *mak2-65* and *cpkA-73*.

2 The arrows indicate the presence/absence of Sch1.

Table 1. Phenotypes of plant pathogenic fungi defective in $G\alpha_i$ protein signalling.

Organism	$G\alpha_i$ gene	Function
Stagonospora nodorum	*Gna1*	Pycnidiation, extracellular protease secretion, DOPA metabolism and virulence
Alternaria alternata	*Aga1*	Conidial germ tube formation and virulence
Botrytis cinerea	*Bcg1*	Vegetative growth, conidiation, extracellular protease secretion and virulence
Cochliobolus heterostrophus	*Cga1*	Appressorium formation and female fertility
Colletotrichum trifolii	*Ctg1*	Vegetative growth, conidia germination and virulence
Cryphonectria parasitica	*Cpg1*	Colony morphology, female fertility, pigmentation, hydrophobin expression and virulence
Fusarium oxysporum	*Fga1*	Conidiation, heat resistance and virulence
Magnaporthe grisea	*MagB*	Vegetative growth, conidiation, appressorium formation, female fertility and virulence

Table 2. Identification of differentially abundant proteins with LC-MS/MS and Mascot.

Spot	Fold diff. [a]	SNOG	Putative identity	Observed; *predicted* pI	Observed; *predicted* M_r (kDa)	*Mowse*; peptide number (% coverage)	Signal peptide	Transcript correlation [b]
C1	-2.7	13042	Short-chain dehydrogenase	5.81; *5.41*	27.1; *28.9*	*748*; 20 (52)	N	Y
C2	-17.5	10217	Short-chain dehydrogenase	5.94; *5.46*	28.5; *31.8*	*696*; 16 (55)	N	Y
C3	-7.2	07541	Proteasome component	6.06; *6.20*	29.2; *27.9*	*256*; 7 (37)	N	N
C4	-3.5	07604	Glutathione transferase	7.43; *6.53*	23.3; *24.4*	*128*; 4 (24)	N	N
C5	-19.2	11081	Concanamycin-induced protein C (CipC)	5.70; *5.21*	<15.0; *15.1*	*386*; 10 (60)	N	Y
C6	+4.7	11441	3-dehydroquinate dehydratase	7.43; *6.49*	<15.0; *16.5*	*223*; 6 (37)	N	Y
C6	+4.7	08275	Unknown	7.43; *6.13*	<15.0; *14.7*	*205*; 6 (44)	N	N

[a] Fold difference of matching protein spots is calculated from normalised spot value of SN15 relative to *gna1-35*; [b] Refer to Fig. 2.

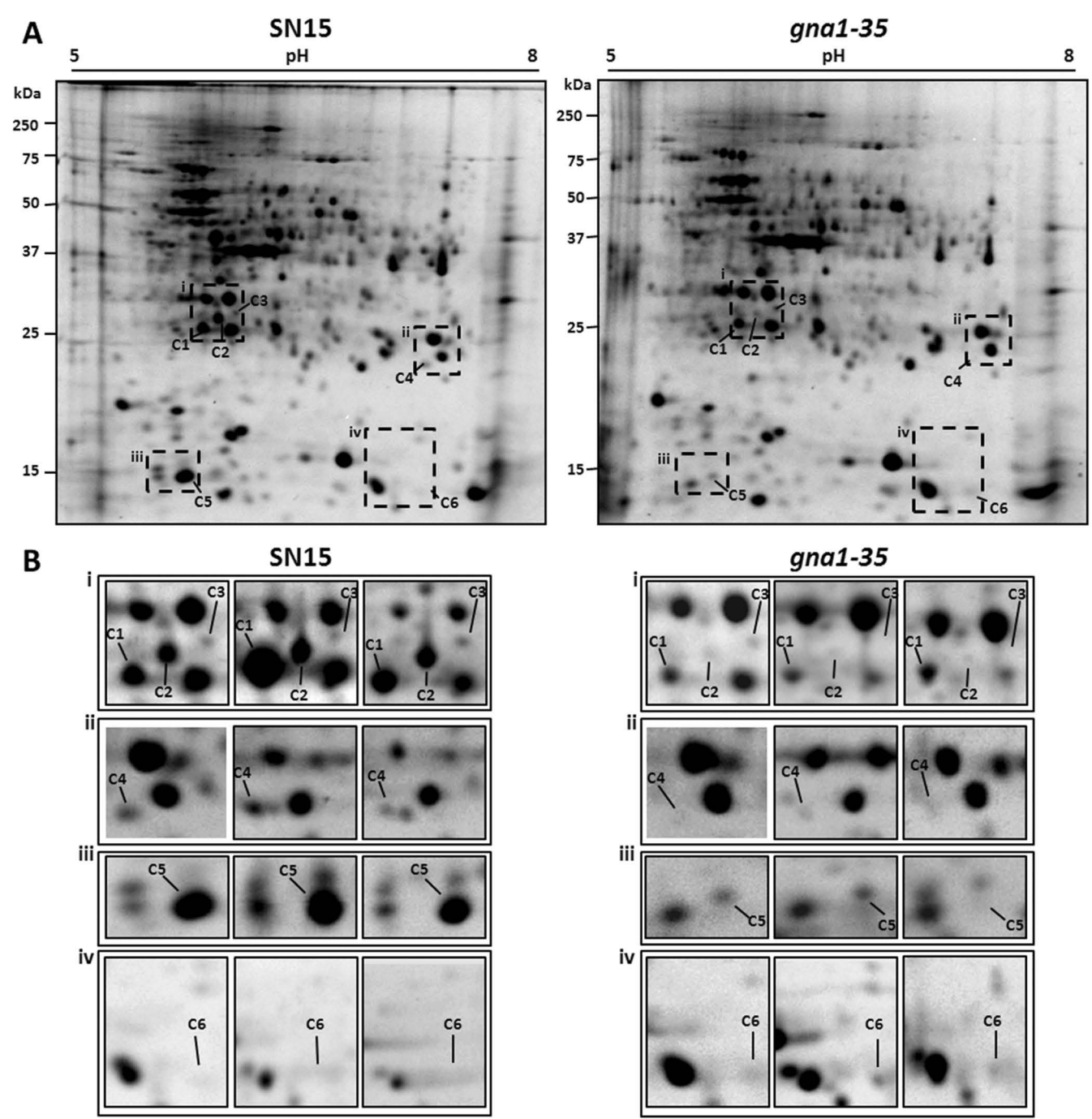
A
SN15
gna1-35
5
pH
8
kDa
250
75
50
37
25
15
i
ii
iii
iv
C1
C2
C3
C4
C5
C6
B
SN15
gna1-35

Figure 2

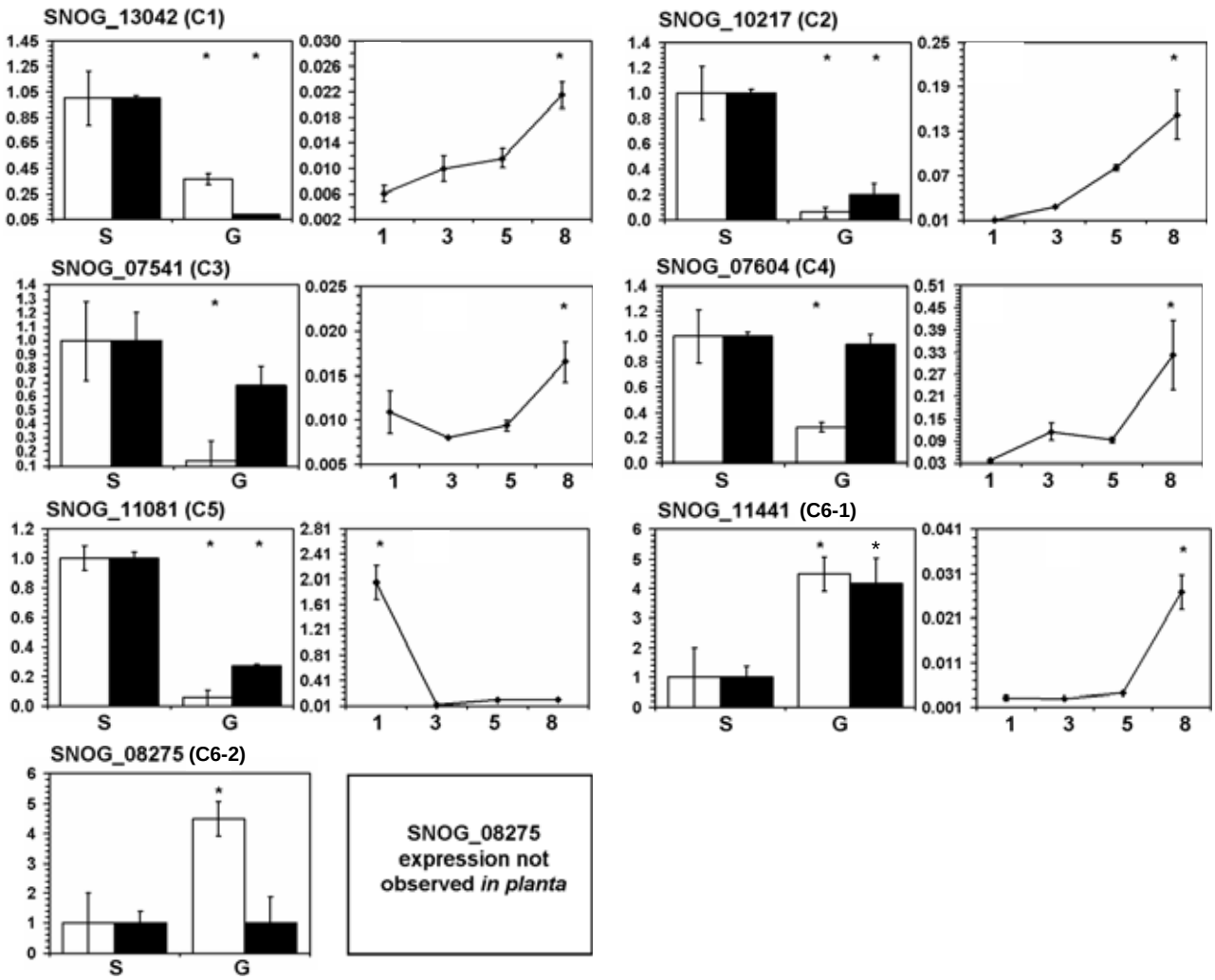
SNOG_13042 (C1)
SNOG_10217 (C2)
SNOG_07541 (C3)
SNOG_07604 (C4)
SNOG_11081 (C5)
SNOG_11441 (C6-1)
SNOG_08275 (C6-2)
S
G
1
3
5
8
SNOG_08275 expression not observed *in planta*

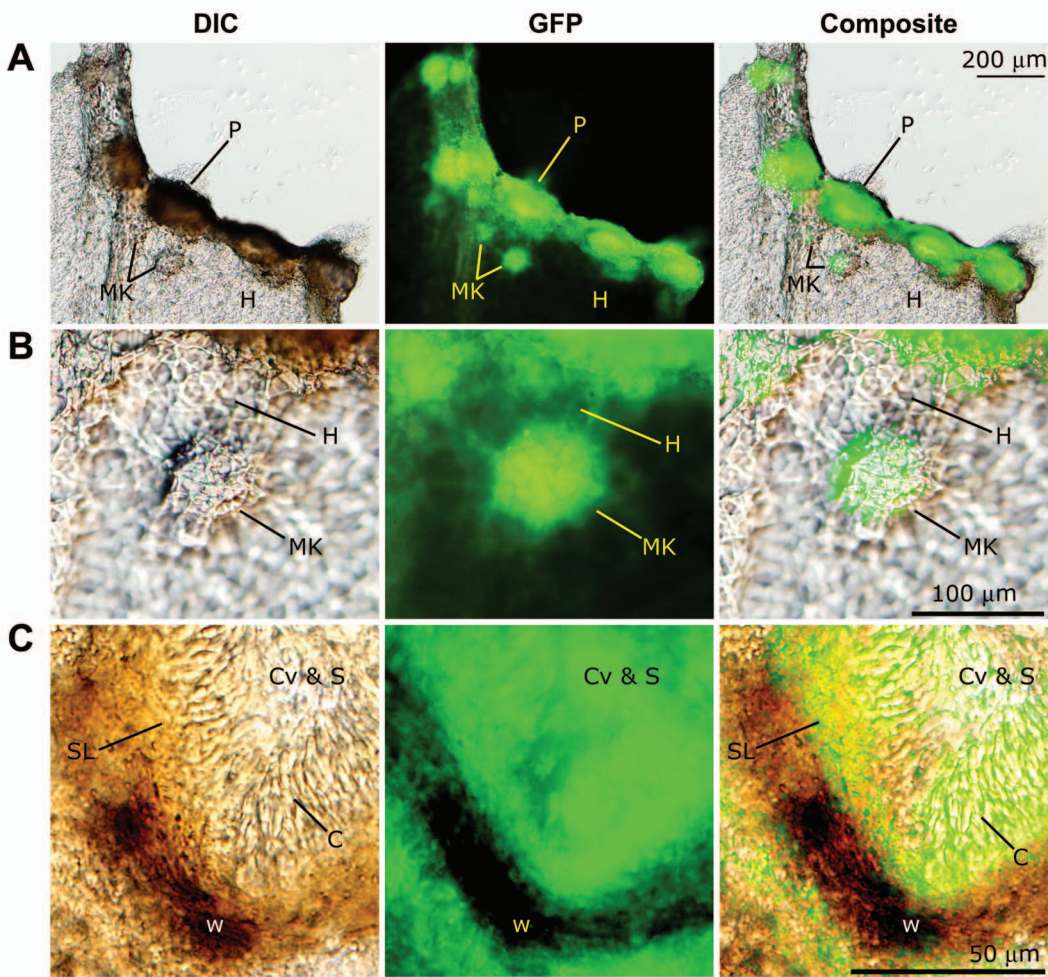
DIC
GFP
Composite
A
B
C
P
MK
H
200 µm
Cv & S
SL
C
W
100 µm
50 µm

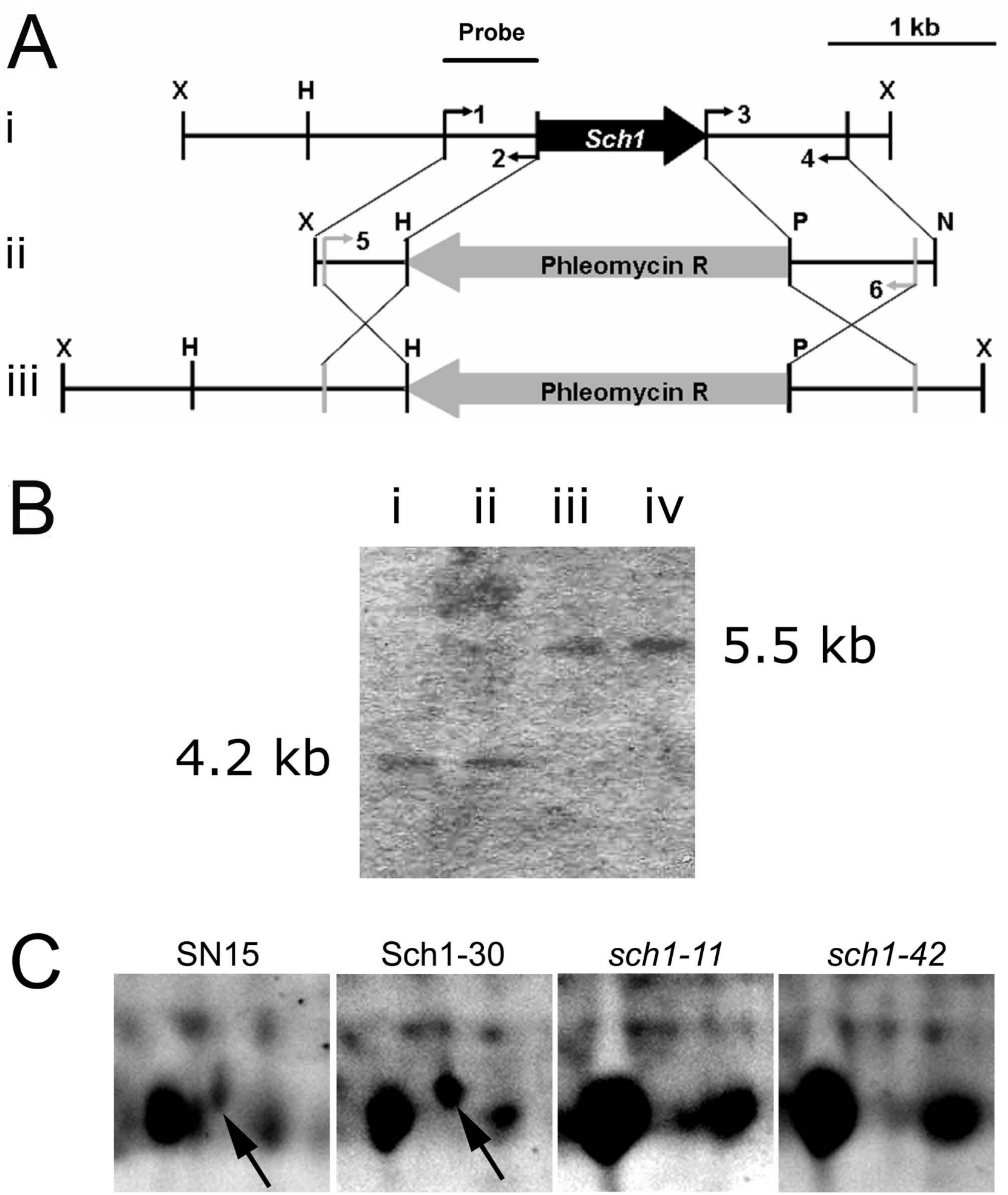
A
Probe
1 kb
i
X
H
1
Sch1
3
X
2
4
ii
X
H
5
P
N
Phleomycin R
6
iii
X
H
H
P
X
Phleomycin R
B
i
ii
iii
iv
4.2 kb
5.5 kb
C
SN15
Sch1-30
sch1-11
sch1-42

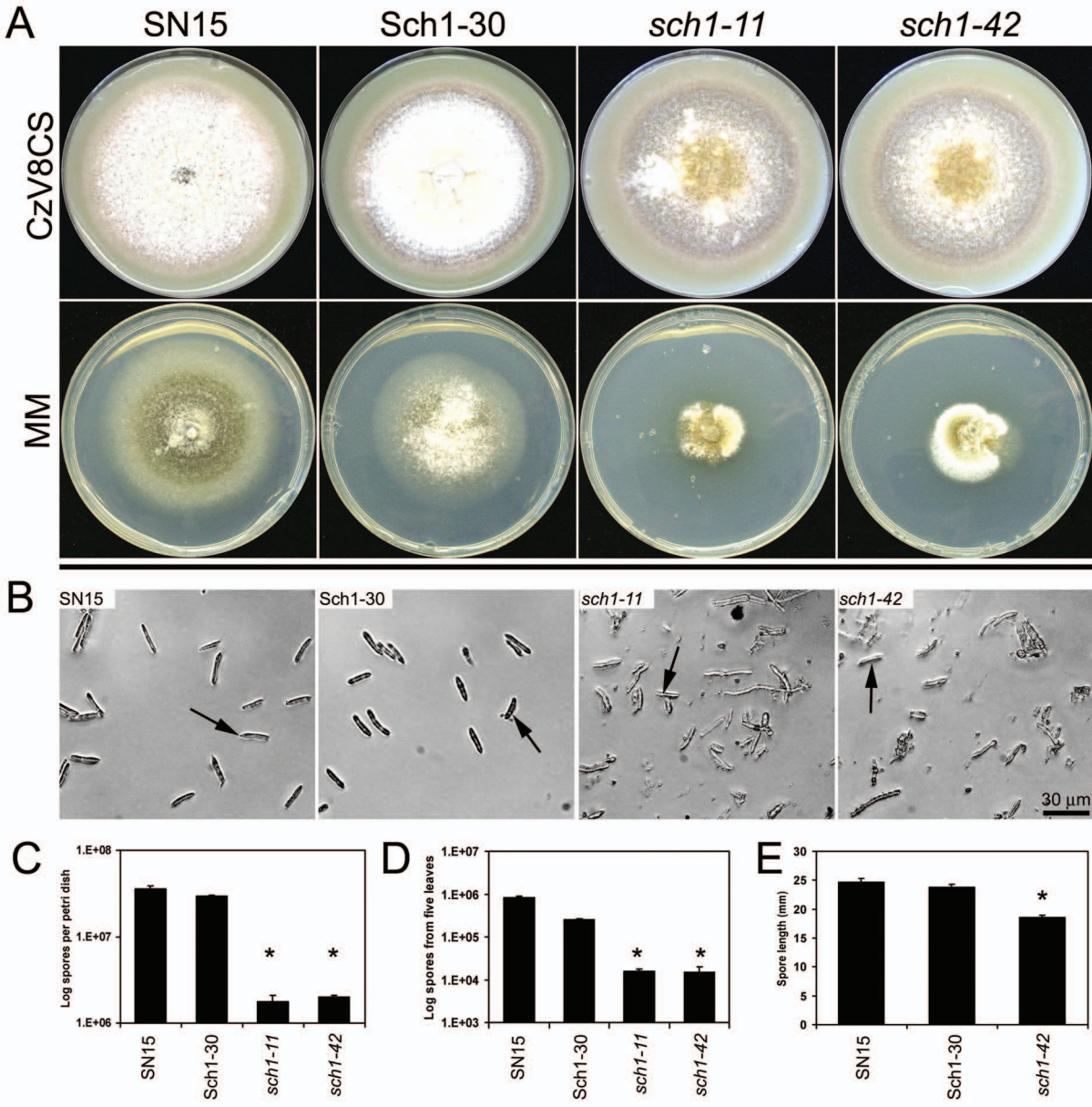
A
SN15
Sch1-30
sch1-11
sch1-42
CzV8CS
MM
B
SN15
Sch1-30
sch1-11
sch1-42
30 μm
C
Log spores per petri dish
1.E+08
1.E+07
1.E+06
SN15
Sch1-30
sch1-11
sch1-42
D
Log spores from five leaves
1.E+07
1.E+06
1.E+05
1.E+04
1.E+03
SN15
Sch1-30
sch1-11
sch1-42
E
Spore length (mm)
30
25
20
15
10
5
0
SN15
Sch1-30
sch1-42

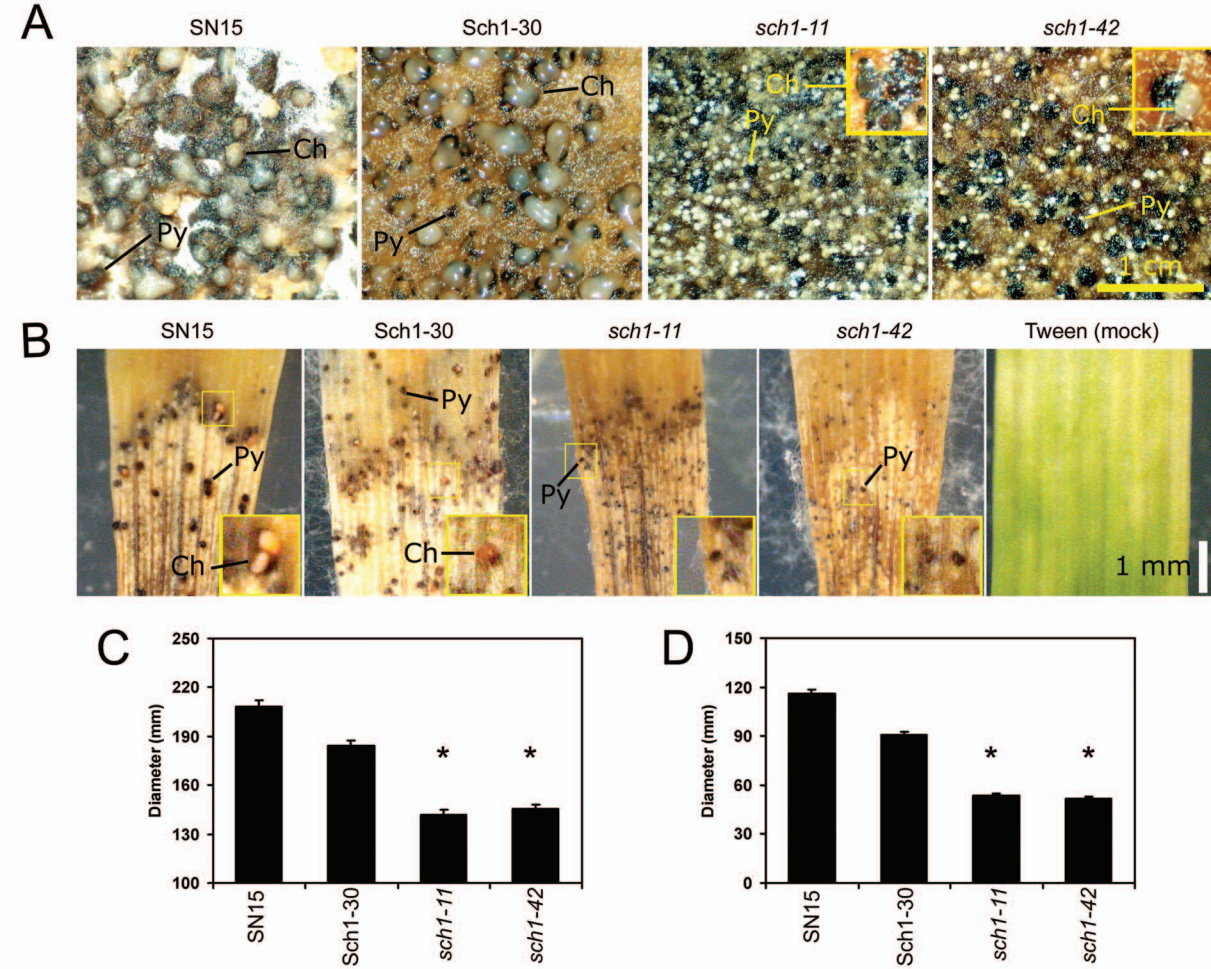
A
SN15
Sch1-30
sch1-11
sch1-42
Ch
Py
1 cm
B
SN15
Sch1-30
sch1-11
sch1-42
Tween (mock)
Py
Ch
1 mm
C
Diameter (mm)
250
220
190
160
130
100
SN15
Sch1-30
sch1-11
sch1-42
*
D
Diameter (mm)
150
120
90
60
30
0
SN15
Sch1-30
sch1-11
sch1-42
*

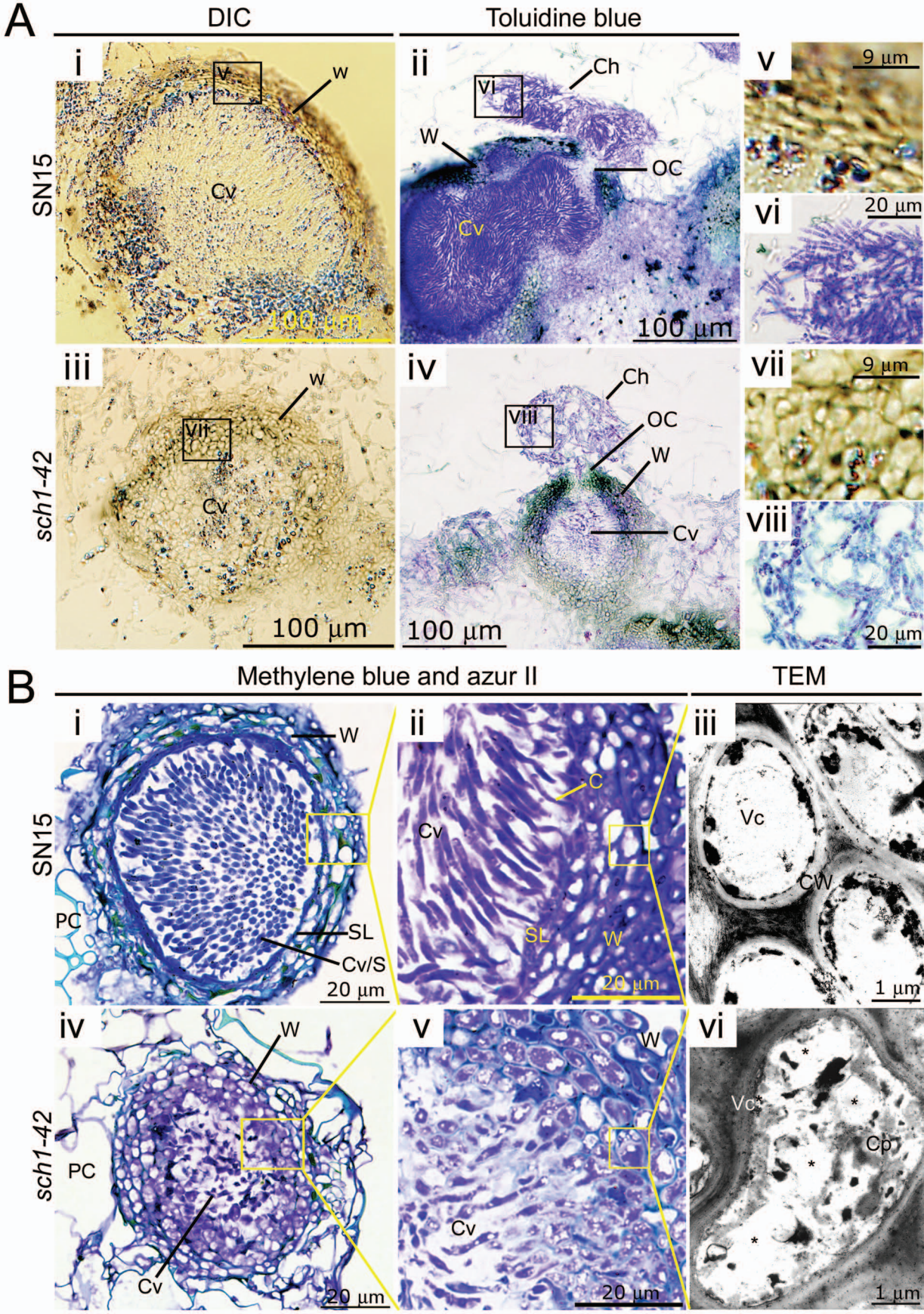
A
DIC
Toluidine blue
i
ii
iii
iv
v
vi
vii
viii
SN15
sch1-42
V
VI
VII
VIII
W
Ch
OC
Cv
100 µm
9 µm
20 µm
B
Methylene blue and azur II
TEM
C
PC
SL
Cv/S
Vc
CW
Cp
1 µm
20 µm

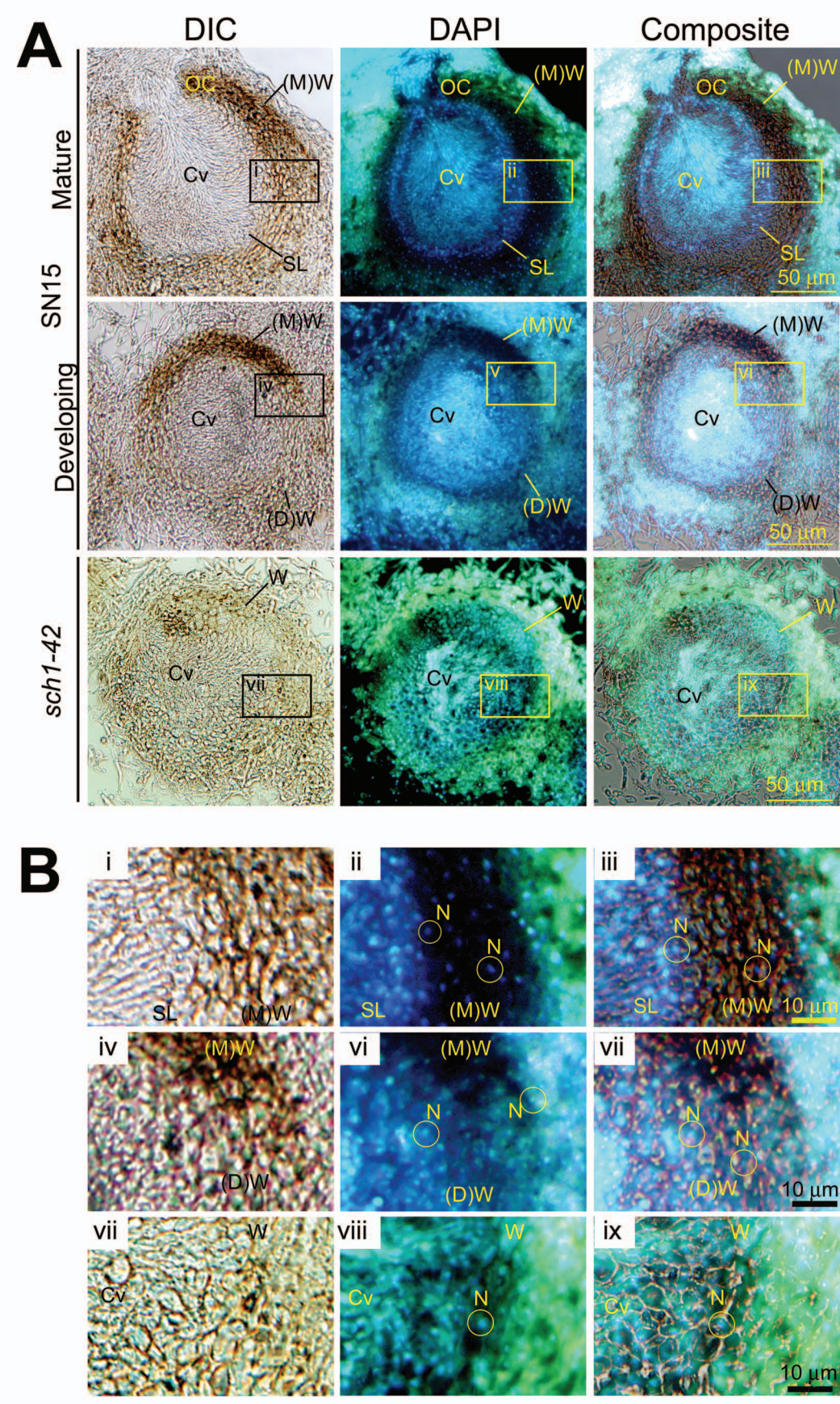
A
DIC
DAPI
Composite
SN15
Mature
Developing
sch1-42
OC
(M)W
Cv
SL
(D)W
W
50 µm
B
N
10 µm

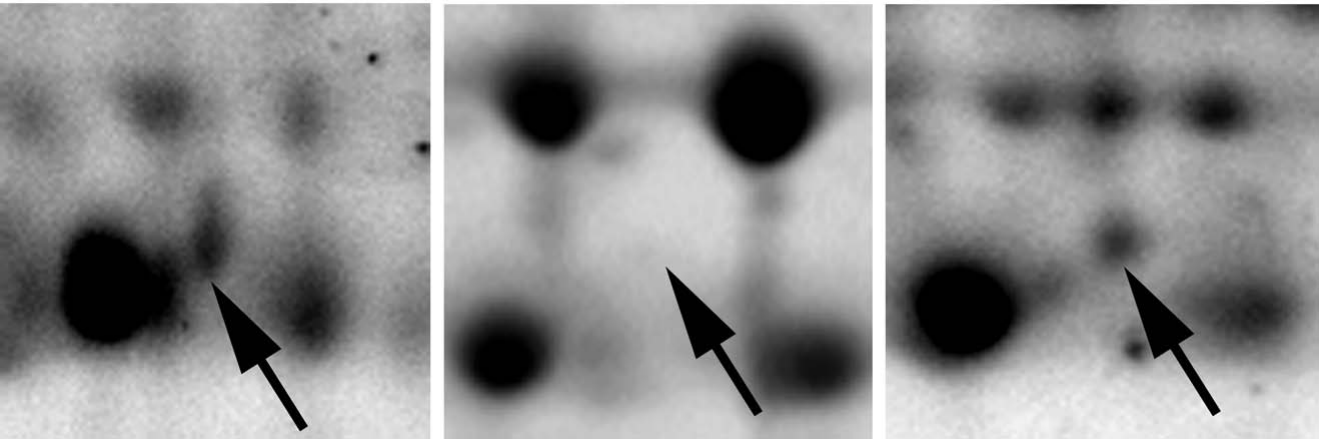
SN15
mak2-65
cpkA-73

Spot	Strain	Normalised protein abundance value			Mean	Standard error	P-value
		Experiment 1	Experiment 2	Experiment 3			
C1	SN15	6.014	2.709	5.199	4.641	0.994	0.044
	SNGna35	1.567	1.421	2.082	1.69	0.2	
C2	SN15	2.189	2.354	3.415	2.653	0.384	0.023
	SNGna35	0.077	0.14	0.238	0.152	0.047	
C3	SN15	0.272	0.716	0.84	0.609	0.172	NA
	SNGna35	0.254	0	0	0.085	0.085	
C4	SN15	0.486	0.41	0.224	0.373	0.078	0.028
	SNGna35	0.131	0.105	0.083	0.106	0.014	
C5	SN15	3.14	4.096	4.074	3.77	0.315	NA
	SNGna35	0.588	0	0	0.196	0.196	
C6	SN15	0.238	0	0	0.079	0.079	NA
	SNGna35	0.297	0.322	0.445	0.355	0.046	

Gene	Primer code	Sequences (5'-3')
Sch1	FP1F01Fwd	CACTCAAGAGTCTTGCCCCATCC
	FP1F01Rev	ATCAGCACATCGATCTTGCCG
Sch1	5'FwdXhoI-R567	CTCGAGATCTACGCCTTGGTCCAGTG
	5'RevHindIII-R567	AAGCTTTAGCTGCGGAGTCGTGATCT
Sch1	3'FwdPstI-R567	CTGCAGGAAGGGCAGATGAGTGTAA
	3'RevNotI-R567	GCGGCCGCTACACATAAACTTAGACTTG
Sch1	R567FwdKO	CCTTGGTCCAGTGGAATCGGA
	R567RevKO	CGACCTCGTCATCGTATGGAAAACT
Sch1	Sch1GFPtransF	AGCCATCGCTTTGTAGGGTC
	Sch1GFPtransR*	TCGCCCTTGCTCACCATTGTAGCTGCGGAGTCGTGAT
EGFP	GFP-PCRf	ATGGTGAGCAAGGGCGA
	GFP-PCRr	GAGCCCGTCACAGAAGATGATA
SNOG_01139	ActinF	CTGCTTTGAGATCCACAT
	ActinR	GTCACCACTTTCAACTCC
SNOG_01139	ActinqPCRf	AGTCGAAGCGTGGTATCCT
	ActinqPCRr	ACTTGGGGTTGATGGGAG
SNOG_07541	R563RTF	CAGCCTCATAACACCTAACATTGGC
	R563RTR	GCTTGTAGCCGGTATGTGAGACCT
SNOG_07604	R646RTF	GTCTGGTTCACGGGCTTCCA
	R646RTR	GAGTACTTGCCGCCGACCAA
SNOG_08275	R800RTF	TATCACAAGTACATCAGC
	R800RTR	GAGAGCGGTTGATGGAAGGCA
SNOG_11081	F6B03rtF1	GGTTTCTGGGATAAGAAC
	F6B03rtR1	TTTAGCCTCAGTCTGAGC
SNOG_11441	R806RTF	GATCACCTTTTCGCACATTCAGTCC
	R806RTR	TTAATGCTCCAGGGTTGATCACAA
SNOG_11663	EF-1alphaF	TGTTGTCGCCGTTGAATC
	EF-1alphaR	CTCATCGTCGCCATCAAC
SNOG_13042	R1048RTF	AGTGACGACGCCAATGTGGC
	R1048RTR	AACTGAGTTCGCGATGCGGG

*underlined sequence is a reverse complement of GFP-PCRf

Comments
RT-PCR
Amplification of 5' *Sch1* UTR for knockout vector construction
Amplification of 3' *Sch1* UTR for knockout vector construction
Amplification of the *Sch1* knockout vector
Amplification of the *Sch1* putative promoter site
Amplification of *eGFP* from pGPD-GFP
Intron spanning PCR
RT-PCR
RT-PCR
RT-PCR
RT-PCR
RT-PCR
RT-PCR
RT-PCR
RT-PCR

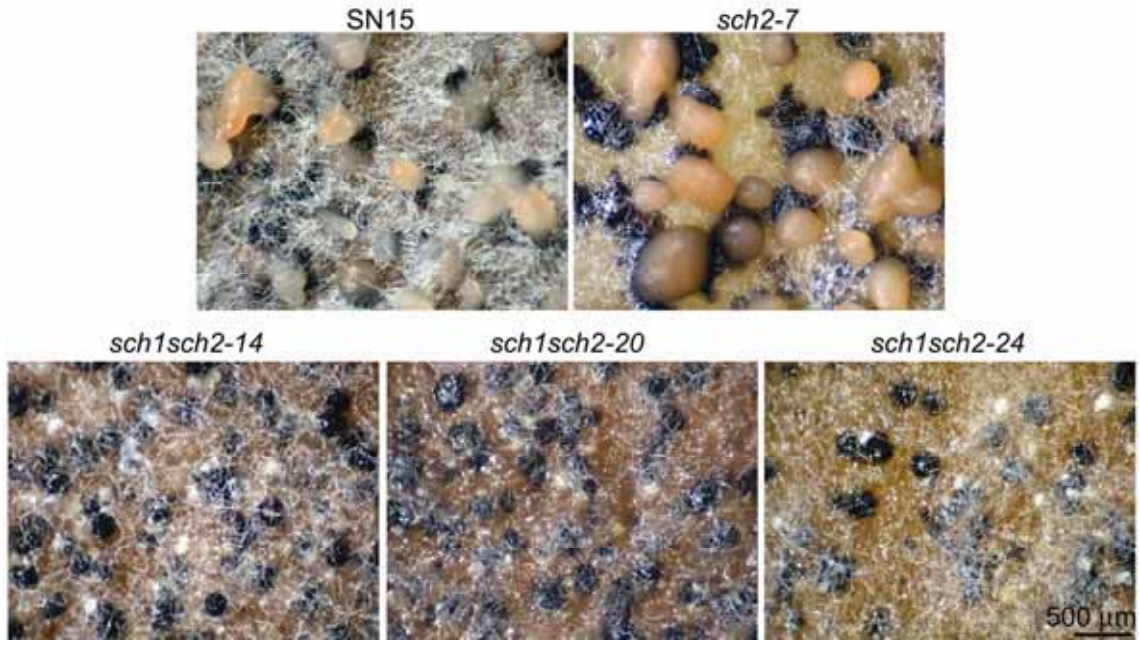

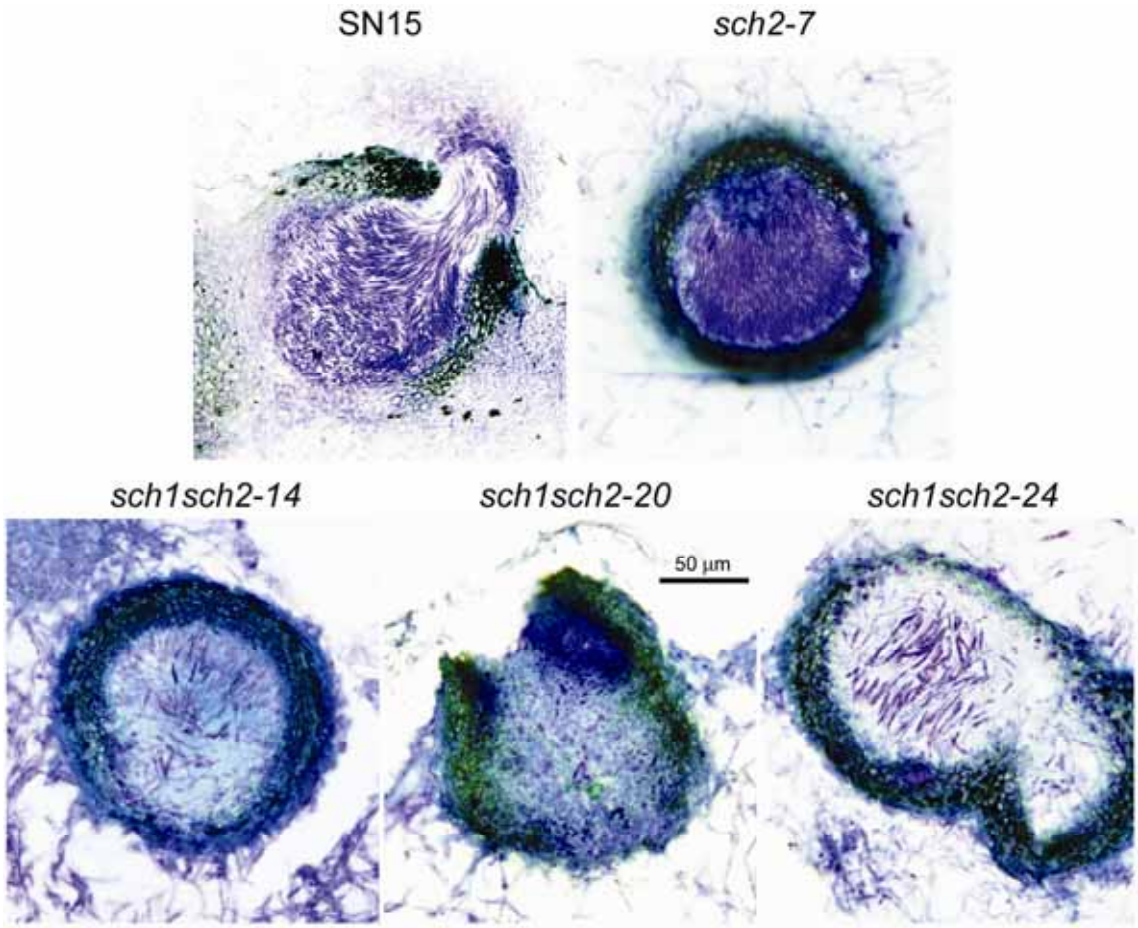

Supplementary Data 3. (A) Stereomicroscope images of pycnidia produced by SN15, *sch2-7* and 3 independently derived *sch1sch2* strains. The images of the double mutants closely match those observed with sch1 strain (Figure 6); (B) Microscopic images of toluidine blue stained sectioned pycnidia of the SN15, *sch2-7* and 3 independently derived *sch1sch2* strains. As in observed in (A), the images of the double mutants closely correlate with the sectioned images of the *sch1* pycnidia (Figure 7).

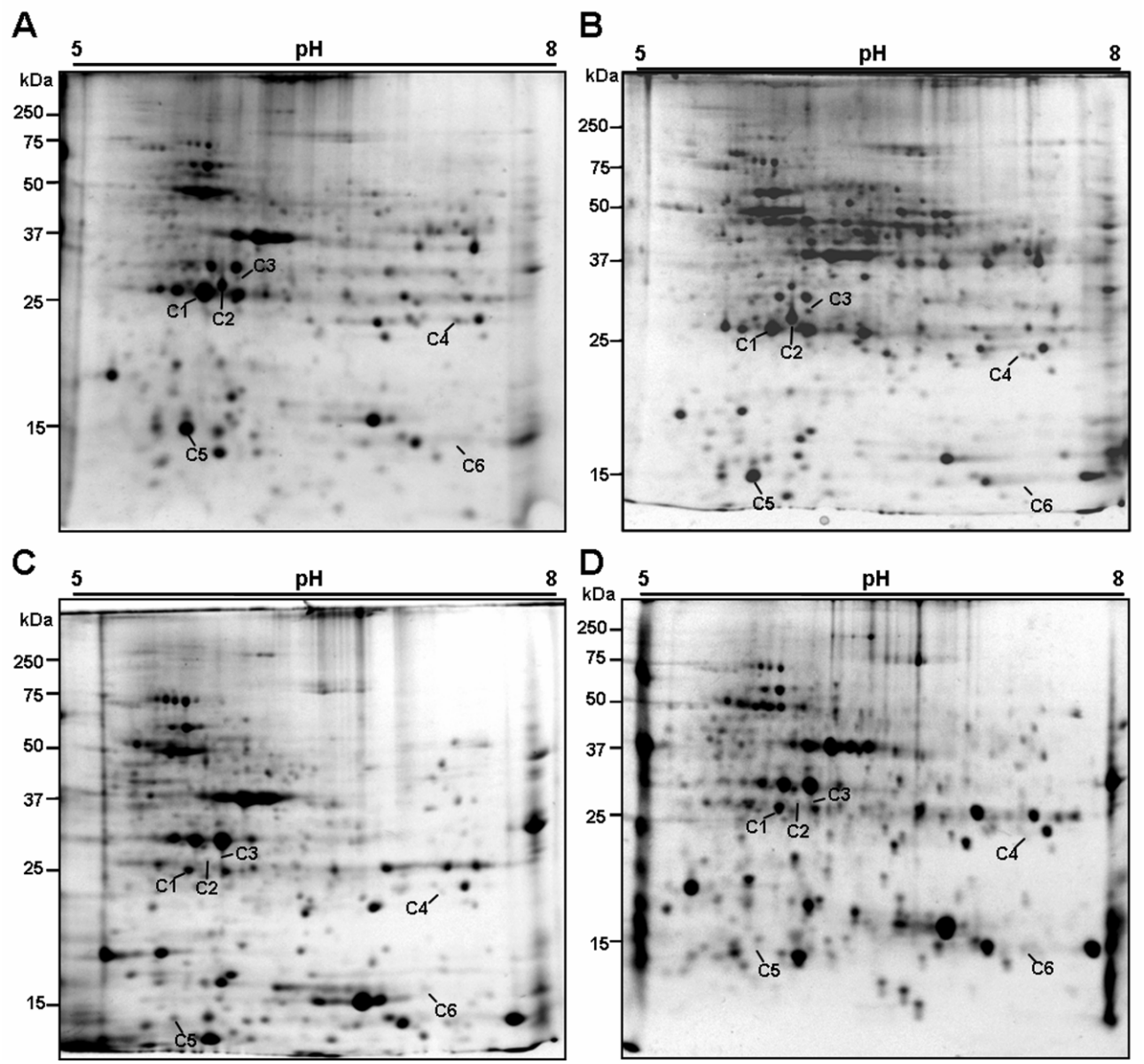

Supplementary Data 3. Replicate 2DE gels of SN15 (A and B) and *gna1-35* (C and D) intracellular proteomes.